Radiation Physics and Chemistry 244 (2026) 113778

Contents lists available at ScienceDirect

Radiation Physics and Chemistry

journal homepage: www.elsevier.com/locate/radphyschem

Non-classical thermoluminescence kinetics and inverse fading behavior in $K_7CaGd_2(B_5O_{10})_3$ phosphor

E. Aymila Cin [a], Kenan Bulcar [b], Abeer S. Altowyan [c,**], M.B. Coban [d], U.H. Kaynar [e,f], O.T. Ozmen [e], Jabir Hakami [g], H. Aydin [h,i], A. Canimoglu [j], Mustafa Topaksu [k], N. Can [g,*]

[a] Bakırcay University, Graduate School of Natural and Applied Sciences, Menemen, Izmir, Türkiye
[b] Igdir University, Vocational School of Health Services, Karaagac Campus, 76000, Igdir, Türkiye
[c] Department of Physics, College of Science, Princess Nourah Bint Abdulrahman University, P.O. Box 84428, Riyadh, 11671, Saudi Arabia
[d] Balikesir University, Faculty of Arts and Sciences, Department of Physics, Balikesir, Turkiye
[e] Bakırcay University, Faculty of Engineering and Architecture, Department of Fundamental Sciences, Menemen, Izmir, Turkiye
[f] Bakırçay University, Biomedical Technologies Design Application and Research Center, Menemen, Izmir, Turkiye
[g] Jazan University, College of Science, Department of Physical Sciences, Physics Division, P.O. Box 114, 45142, Jazan, Kingdom of Saudi Arabia
[h] Central Research Laboratories, Izmir, Katip Celebi University, Turkiye
[i] Graphene Application&Research Center, Izmir, Katip Celebi University, Turkiye
[j] Omer Halisdemir University, Faculty of Arts and Sciences, Physics Department, Nigde, Turkiye
[k] Physics Department, Cukurova University, Arts-Sciences Faculty, 01330, Adana, Türkiye

ARTICLE INFO

Handling Editor: Dr. Chris Chantler

Keywords:
$K_7CaGd_2(B_5O_{10})_3$
Thermoluminescence
Borate phosphors
Inverse fading
Anomalous heating-rate effects

ABSTRACT

The thermoluminescence (TL) properties of the newly synthesized $K_7CaGd_2(B_5O_{10})_3$ phosphor were systematically investigated to assess its potential for dosimetric applications. A prominent TL peak near 220 °C was observed, accompanied by additional features indicating a complex trap structure. Activation energies were calculated using variable heating rate (VHR) methods, including refined Hoogenstraaten and Booth–Bohun–Parfianovitch approaches, with corrections applied for thermal lag to improve accuracy. VHR analysis of the dominant dosimetric peak yielded activation energies consistent with an apparent first-order approximation, as evidenced by the linearity of the corrected kinetic plots. T_m–T_{stop} and initial rise (IR) methods revealed thirteen discrete trap levels with activation energies ranging from 1.17 to 2.09 eV. Complementary computerized glow curve deconvolution (CGCD) analysis provided a fitting-based decomposition consistent with this rich trap distribution: thirteen overlapping TL peaks were resolved before preheating, with frequency factors up to $\sim 10^{17}$ s^{-1}, which may be consistent with the presence of spatially correlated trapping and recombination centers. Following preheating, thermally unstable shallow traps were removed, isolating eight stable peaks (E_a = 1.21–2.09 eV), and demonstrating the effectiveness of thermal treatment in enhancing signal stability. The phosphor showed a linear dose–response over the range of 1.4–30.1 Gy, indicating stable behaviour within the investigated mid-dose region. A reproducible increase of approximately a 20-fold enhancement in TL signal was observed within 12 h of storage under controlled laboratory conditions, deviating from classical fading behaviour. This trend may represent an inverse fading–like response, potentially driven by delayed recombination, quantum mechanical tunnelling, or charge redistribution among metastable trap configurations. Despite the near-first-order behaviour of the main dosimetric peak, the overall TL response exhibited non-classical characteristics, including heating-rate-dependent intensity enhancement (0.1–10 °C/s) and time-dependent signal amplification. These observations suggest that, while the dominant trap behaves quasi-independently under standard kinetic evaluation, the broader trapping–recombination system likely involves semi-localized or dynamically evolving recombination processes. Overall, these findings demonstrate that $K_7CaGd_2(B_5O_{10})_3$ exhibits structurally rich and thermally stable trapping characteristics within the investigated β-dose regime. However, further studies addressing low-dose response, photon-energy dependence, and comparison with established dosimetric standards are required before broader practical applications can be considered.

* Corresponding author.
** Correspondimg author.
E-mail addresses: asaltowyan@pnu.edu.sa (A.S. Altowyan), ncan@jazanu.edu.sa (N. Can).

https://doi.org/10.1016/j.radphyschem.2026.113778
Received 28 December 2025; Received in revised form 23 February 2026; Accepted 5 March 2026
Available online 6 March 2026
0969-806X/© 2026 Elsevier Ltd. All rights are reserved, including those for text and data mining, AI training, and similar technologies.

1. Introduction

Thermoluminescence (TL) research in insulating materials has evolved significantly since early models treated defect sites as simple, localized anomalies in perfect crystal lattices. However, extensive experimental evidence from optical absorption, electron paramagnetic resonance (EPR), and TL spectroscopy indicates that defect sites, particularly in complex oxides and borates, interact with their surrounding lattice environments (Grachev and Deĭgen, 1978; Hayes and Stoneham, 2014; Townsend and Wang, 2024). These findings call for a reassessment of the purely point-defect-based descriptions, especially in structurally complex powder materials (Townsend and Wang, 2024).

Boron-based hosts provide wide band gaps and structurally flexible frameworks suitable for thermoluminescence studies (Dorenbos, 2003; McKeever, 1985; Yin et al., 2023). Several borate compounds such as $YBa_3(BO_3)_3$, $K_7SrY_2(B_5O_{10})_3$, $GdCa_4O(BO_3)_3$, and $Ca_4YO(BO_3)_3$ have been reported to exhibit strong TL and persistent luminescence properties, especially when doped with rare-earth ions like Dy^{3+}, Eu^{3+}, Sm^{3+} or Tb^{3+} (Alathlawi et al., 2025; Bulcar et al., 2025; Çin et al., 2026; Madkhli et al., 2024; Souadi et al., 2025). These studies highlight the role of the borate matrix in supporting efficient trap formation and recombination mechanisms. While structurally related borate phosphors have been extensively investigated, most studies emphasize conventional glow-curve analysis and standard kinetic parameter extraction. However, the intrinsic TL of undoped complex borates is still poorly understood, although they may host native traps linked to lattice irregularities and structural disorder. In this context, the compound $K_7CaGd_2(B_5O_{10})_3$ presents a structurally rich and chemically diverse system, incorporating both alkaline (K^+, Ca^{2+}) and rare-earth (Gd^{3+}) ions into a borate matrix of considerable complexity.

To our knowledge, no TL studies have been conducted on $K_7CaGd_2(B_5O_{10})_3$ in either doped or undoped form. However, the novelty of the present work does not reside solely in examining a previously unreported composition. The known influence of Gd^{3+} ions on TL behaviour, primarily through their role in intrinsic defect formation, spin–orbit coupling, and efficient energy transfer, makes this host particularly suitable for probing complex trapping dynamics. TL studies on Gd_2O_3 -based materials (e.g., Gd_2O_3:Eu^{3+} and Gd_2O_3:Er^{3+}) have shown strong glow peaks and long-lasting luminescence under UV light, highlighting the role of the Gd^{3+} lattice in supporting trap-assisted recombination (Hai et al., 2018). Additionally, low-temperature TL measurements on undoped Gd_2O_3 nanoparticles revealed well-defined glow curves and activation energies, confirming that Gd^{3+}-rich lattices can support thermally stimulated charge release in the absence of activator ions (Delice et al., 2019). In this study, no direct structural or spectroscopic measurements of defect clustering, grain boundaries, or adsorbed water are performed; such mechanisms are therefore considered only at a qualitative level to contextualize the observed kinetic behaviour.

These findings suggest that Gd^{3+}-containing borate hosts—such as $K_7CaGd_2(B_5O_{10})_3$ —may exhibit measurable TL behaviour through native trap states associated with local lattice distortions and defect clustering. Furthermore, the powder morphology introduces additional complexity: surface water adsorption, nanoparticle inclusions, and grain-boundary defects have all been shown to influence trapping and recombination kinetics in unexpected ways (Townsend and Wang, 2024; Yang et al., 1998). Although these factors have been discussed in the broader TL literature, the present study does not directly probe their microscopic contributions. They are therefore mentioned only as possible contextual influences rather than experimentally verified mechanisms in $K_7CaGd_2(B_5O_{10})_3$.

Accordingly, the present work provides a comprehensive TL investigation of undoped $K_7CaGd_2(B_5O_{10})_3$, with particular emphasis on identifying non-classical kinetic behaviour beyond conventional first- and second-order descriptions. The discussion therefore focuses primarily on phenomenological kinetic behaviour (e.g., inverse fading and anomalous heating-rate dependence), while possible defect scenarios are mentioned only in a contextual sense informed by the broader TL literature. In this context, inverse fading—characterized by a post-irradiation increase in luminescence intensity—has been reported in NaCl-based TL and OSL systems and has been increasingly recognized as a rare but physically meaningful non-classical relaxation phenomenon rather than an experimental artefact (Waldner and Bernhardsson, 2018; Ekendahl et al., 2025). Similar time-dependent signal enhancement has also been observed in α-Al_2O_3:C, where the main TL peak was reported to increase systematically during storage under controlled laboratory conditions, and was attributed to charge redistribution or hopping between competing trap states (Kalita and Chithambo, 2017a). Furthermore, sensitivity evolution studies in α-Al_2O_3:C and α-Al_2O_3:C, Mg have demonstrated that trap populations can evolve during repeated irradiation–readout cycles, leading to measurable intensity enhancement (Kalita and Chithambo, 2017b). Although these materials differ structurally from complex borate hosts and are typically dominated by F-centre–related defects, the phenomenological similarity suggests that delayed recombination or redistribution among metastable trap configurations may represent a more general, though still relatively rare, TL behaviour.

In addition to conventional glow-curve and kinetic analyses, this study specifically investigates two atypical behaviours rarely examined within this borate structural family: anomalous heating-rate dependence and time-dependent TL enhancement (inverse fading–like behaviour). The former refers to deviations from the heating-rate-dependent activation energy trends commonly expected under general-order kinetics, indicating the presence of complex carrier dynamics or overlapping trap–recombination pathways. The latter, manifested as an increase in TL signal intensity during post-irradiation storage, suggests non-classical charge relaxation processes, such as delayed recombination or thermally assisted charge redistribution. Thus, the novelty of this work lies not solely in the examination of a previously unreported host composition, but in the systematic analysis of inverse fading and non-classical TL kinetics in an undoped $K_7CaGd_2(B_5O_{10})_3$ system. Together, these observations motivate the need for kinetic descriptions that extend beyond conventional first- and second-order TL models, and establish $K_7CaGd_2(B_5O_{10})_3$ as a suitable model system for probing complex trapping phenomena in powder phosphors.

2. Experiment

2.1. Synthesis of undoped $K_7CaGd_2(B_5O_{10})_3$ powders

Nanocrystalline powders of $K_7CaGd_2(B_5O_{10})_3$ (abbreviated as KCGBO) were synthesized via a sol–gel-assisted microwave combustion route. All precursor chemicals were of analytical grade and used without further purification. Gadolinium (III) oxide (Gd_2O_3, Sigma-Aldrich, 99.99%) was first dissolved in dilute nitric acid (1 N) under mild heating to obtain a clear Gd^{3+} nitrate solution. Subsequently, stoichiometric amounts of potassium nitrate (KNO_3, ≥99.0%), calcium nitrate tetrahydrate ($Ca(NO_3)_2{\cdot}4H_2O$, ≥99.5%), and boric acid (H_3BO_3, ≥99.5%) were added to the solution in accordance with the target molar composition of the KCGBO host. Urea (CH_4N_2O) and glycine ($C_2H_5NO_2$) were used as organic fuels to promote the combustion reaction. Deionized water (20 mL) was introduced to aid homogenization, and the mixture was stirred magnetically at 80 °C for 1 h until a transparent, viscous gel was formed. Gelation occurred after partial evaporation of the solvent, yielding a thick and uniformly dispersed sol matrix suitable for combustion. The prepared gel was then transferred to a domestic microwave oven (2.45 GHz, 800 W) and irradiated for approximately 6–8 min. Rapid gas evolution and spontaneous ignition indicated the onset of a vigorous combustion reaction, leading to the formation of voluminous, white, foamy powders. The as-synthesized product was collected without further washing. To improve crystallinity and remove residual carbonaceous content, the resulting powders were calcined in

air at 920 °C for 4 h in an alumina crucible. The final product was a fine, white nanocrystalline powder of undoped KCGBO, stored in a desiccator to prevent moisture uptake prior to TL characterization.

2.2. Thermoluminescence measurements

TL measurements were performed using a *Lexsyg Smart TL/OSL reader* (Freiberg Instruments, Germany), housed at Bakircay University, and equipped with a built-in $^{90}Sr/^{90}Y$ beta source calibrated to deliver a nominal dose rate of ~1.436 Gy/s. The nominal dose rate was taken from the manufacturer's calibration certificate of the built-in $^{90}Sr/^{90}Y$ source traceable to a secondary standards dosimetry laboratory with an expanded uncertainty of ±3% (k = 2) at the reference calibration date (October 27, 2025). Samples of 20 ± 2 mg were weighed and uniaxially pressed under an applied pressure of 2000 kgf·cm^{-2} (≈196 MPa) for 10 min to produce pellets with a diameter of 6.00 mm and a thickness of approximately 0.75 mm. This step was carried out to ensure consistent sample geometry and improve thermal contact during heating.

The irradiated samples were heated from room temperature up to 450 °C under a linear heating regime. A standard heating rate of 2 °C/s was used for initial glow curve acquisition. To investigate the influence of thermal ramping on trap dynamics and peak shapes, additional measurements were conducted at varied heating rates ranging from 0.1 °C/s to 10 °C/s. All experiments were conducted under continuous nitrogen flow to prevent surface oxidation and suppress spurious chemiluminescence signals. All thermoluminescence measurements were carried out under standard air-conditioned laboratory conditions, i.e. room temperature and ambient humidity, without any intentional temperature or humidity cycling during storage. TL readout was performed using a Lexsyg Smart TL/OSL reader under continuous nitrogen flow to prevent surface oxidation and suppress spurious chemiluminescence signals. After calcination, the $K_7CaGd_2(B_5O_{10})_3$ powders were stored in a desiccator to minimize moisture uptake prior to TL characterization. Irradiated samples were kept in opaque containers and handled under red-light conditions until the point of measurement to avoid unintended light exposure and premature trap depopulation.

The temperature scale of the Lexsyg Smart reader was verified using the manufacturer's built-in Ni-foil calibration routine, ensuring agreement within ±1 °C over the range 50–450 °C. For variable heating-rate experiments, the effective temperature lag between the heater and the sample was evaluated by analysing peak shifts as a function of heating rate and corrected according to the procedure of Kitis and Tuyn (1998). The validity of the correction was confirmed by improved linearity of the kinetic plots after lag compensation. Following correction, the residual uncertainty in T_m was estimated to be less than ±2 °C across the investigated heating-rate range.

Background subtraction was applied systematically to each glow curve using control data acquired from non-irradiated samples measured under identical conditions. Special care was taken to minimize premature trap depopulation: irradiated samples were stored in opaque containers and handled under red-light conditions until the point of measurement. To further enhance measurement reproducibility and reduce signal noise potentially caused by uneven particle packing, the powders were lightly homogenized in an agate mortar prior to pellet pressing.

This protocol allowed for precise characterization of TL features inherent to the undoped KCGBO matrix, forming a consistent basis for subsequent kinetic modeling and trap parameter analysis.

3. Thermoluminescence analyses

3.1. X-ray diffraction and FTIR analysis of undoped $K_7CaGd_2(B_5O_{10})_3$

Powder X-ray diffraction (XRD) analysis was conducted to confirm the phase purity and crystallographic identity of the undoped KCGBO host. As shown in Fig. 1, all major diffraction peaks are consistent with the standard pattern reported in JCPDS Card No. 04-024-1070, which corresponds to a trigonal system with R32 space group symmetry. The observed reflections match well with those expected for KCGBO -type borates, indicating successful formation of the target phase. The absence of any impurity peaks within the detection limit confirms the single-phase nature of the synthesized material. This result further suggests that the synthesis route yields a homogenous product without residual secondary borate or oxide phases, which could otherwise interfere with subsequent optical analyses. The diffraction pattern exhibits sharp and well-defined Bragg peaks, indicative of good crystallinity in the as-synthesized powder. Notably, the presence of reflections such as (221), (312), and (404) confirms the long-range ordering of the $[B_5O_{10}]$ polyanionic units, which are characteristic of this structural family. No pronounced peak broadening beyond instrumental contributions is observed, suggesting that the crystallites possess adequate structural coherence at the XRD scale. The good agreement between the measured diffraction pattern and the standard reference supports the assignment of a stable trigonal borate framework composed of isolated polyborate clusters interconnected by Ca^{2+} and Gd^{3+} ions. The presence of multiple cations (K^+, Ca^{2+}, Gd^{3+}) reflects the compositional complexity of the host lattice. The existence of multiple trapping states discussed in this work is inferred from thermoluminescence measurements and kinetic analyses rather than directly from structural data.

Rietveld refinement was performed to quantitatively assess the structural model and lattice parameters of the undoped $K_7CaGd_2(B_5O_{10})_3$ phase. The refined unit cell parameters ($a = 13.32902$ Å, $b = 13.32902$ Å, $c = 15.06382$ Å; $\alpha = \beta = 90°$, $\gamma = 120°$) are consistent with a trigonal crystal system (R32 space group) and are in good agreement with the reference data. The refinement indicators ($R_p = 0.0479$, $R_{wp} = 0.0737$, $R_{exp} = 0.0281$, $\chi^2 = 2.623$) indicate satisfactory agreement between the observed and calculated diffraction patterns. The relatively low R-factors and acceptable goodness-of-fit value confirm the reliability of the structural assignment and further support the phase purity of the synthesized material.

The vibrational characteristics of the undoped KCGBO sample were investigated using Fourier-transform infrared (FTIR) spectroscopy in order to probe the local bonding configurations and lattice vibrational behavior. The resulting spectra reveal the characteristic signatures of the $[B_5O_{10}]$ structural units, indicating that the fundamental borate framework is preserved in the synthesized undoped $K_7CaGd_2(B_5O_{10})_3$ structure. The FTIR spectra (Fig. 1b) exhibit a series of distinct absorption bands spanning the range from 400 to 1600 cm^{-1}, which are attributed to the internal vibrational modes of borate groups. The broad absorption band centered around 1425 cm^{-1} is associated with the stretching vibrations of trigonal $[BO_3]$ units. Additional bands observed at 1354, 1243, and 1196 cm^{-1} are assigned to asymmetric B–O stretching modes in distorted $[BO_3]$ units [Terashima et al., 1997]. Prominent absorption features appearing near 1027 and 931 cm^{-1} correspond to the stretching vibrations of tetrahedral $[BO_4]$ units, confirming the simultaneous presence of three- and four-coordinated boron species within the structure. At lower wavenumbers, bands located at approximately 783, 731, 614, 559, and 494 cm^{-1} are attributed to B–O–B bending and in-plane deformation modes associated with the interconnected $[B_5O_{10}]$ polyborate network [Morsy et al., 2025; Ton et al., 2025]. These spectral features and their assignments are in good agreement with previously reported FTIR studies of related borate phosphors, including $K_7CaR_2(B_5O_{10})_3$ and analogous mixed borate systems [Tawalare 2022; Kuznetsov et al., 2019].

3.2. Band filter selection

To resolve the spectral characteristics of TL emission in KCGBO, preliminary tests were conducted using bandpass filters centered at BSL/TL-365 nm, IRSL/TL-410 nm, and IRSL-TL-565 nm (Fig. 2). Among these, the BSL/TL-365 nm filter produced the highest emission intensity and signal-to-noise ratio, indicating that near-UV emission dominates

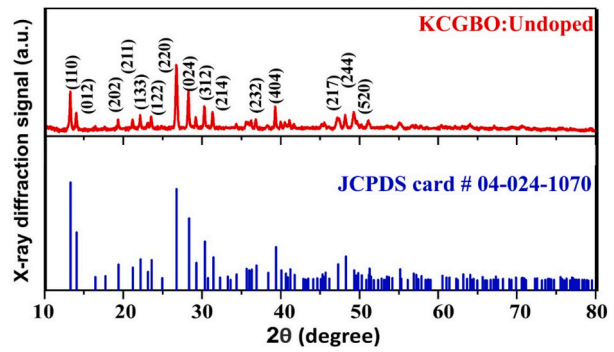

(a)

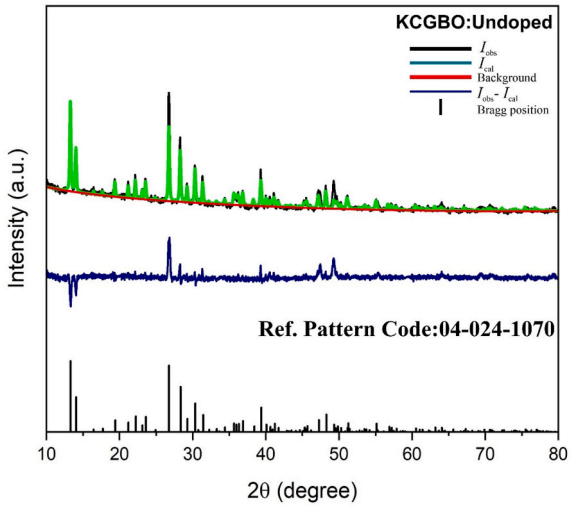

(b)

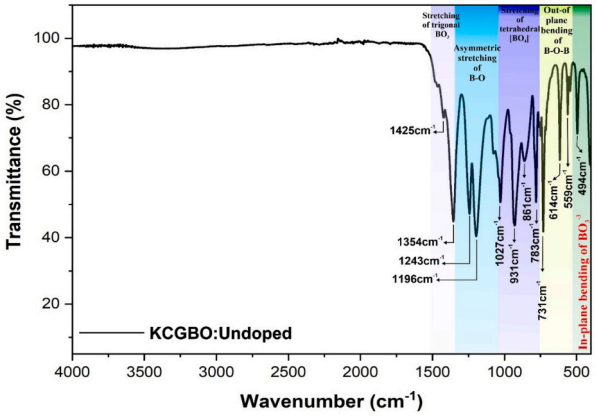

(c)

Fig. 1. (a) X-ray diffraction pattern of undoped KCGBO compared with the standard reference data (JCPDS No. 04-024-1070), confirming phase purity and crystallographic match. (b) Rietveld refinement profile of undoped KCGBO, showing the observed intensities (I_{obs}), calculated pattern (I_{cal}), fitted background, and the difference curve ($I_{obs} - I_{cal}$), along with the Bragg reflection positions. (c) FTIR transmittance spectra of undoped $K_7CaGd_2(B_5O_{10})_3$ phosphors exhibiting characteristic vibrations of trigonal [BO_3] and tetrahedral [BO_4] units.

the intrinsic recombination processes in the undoped host. Based on this observation, all subsequent TL measurements and kinetic analyses in this study were conducted using the BSL/TL-365 nm bandpass filter (FWHM ≈ 10 nm). This filter enables selective detection of the dominant UV emission component while effectively suppressing visible-light contributions and thermal background. Its spectral selectivity aligns with previous studies employing narrow-band TL detection systems for oxide phosphors and borate-based hosts (Bakr et al., 2020). Glow curves were plotted on double logarithmic axes (log–log scale) to better visualize intensity variations spanning multiple orders of magnitude. This representation is especially beneficial when analyzing complex trapping systems, where deep or sparsely populated traps manifest as weak shoulders or tail features in the glow curve. The log–log display enhances the analytical visibility of such features, which may be overlooked on linear or semi-log plots. Moreover, this plotting strategy has been shown to improve the resolution of overlapping peaks and to assist in identifying deviations from first-order kinetics, particularly in powder-based materials with structural disorder (Can et al., 2025).

3.3. *Preheating optimization for TL signal stabilization*

In TL measurements, the presence of unstable shallow traps often leads to low-temperature signal contributions that can obscure the identification of kinetically meaningful peaks. To address this, a preheating step is typically employed to selectively empty these unstable traps prior to glow curve acquisition, thereby enhancing both spectral clarity and kinetic reliability (McKeever, 1985; Peng et al., 2021; Yukihara et al., 2022). In this work, the preheating protocol was systematically optimized by varying both temperature and duration, aiming to eliminate unstable shallow traps while preserving deeper, kinetically significant centers. To establish suitable preheating conditions for undoped $K_7CaGd_2(B_5O_{10})_3$, TL glow curves were recorded after β-irradiation at 20.1 Gy under controlled preheat steps. The reference glow curve obtained without any thermal treatment (Fig. 3a) displays broad emission features below ~150 °C, indicative of a substantial population of shallow traps contributing to the low-temperature background. A systematic heating protocol was then applied in which samples were heated to preselected temperatures between 50 °C and 200 °C (in 5 °C increments) at 2 °C/s, held briefly, and then rapidly cooled to room temperature. Residual TL signals were subsequently recorded upon reheating the sample up to 450 °C. The integrated TL intensity was plotted against preheat temperature (Fig. 3b). A sharp decline in signal was observed between 50 °C and 145 °C, after which the rate of intensity decrease was significantly reduced. This behaviour does not correspond to a true intensity plateau; rather, it marks a transition to a reduced-slope regime dominated by deeper and more thermally stable trapping centers. Based on this trend, 145 °C was selected as the optimum preheat temperature for this host matrix. Preheating to higher temperatures led to a gradual reduction of the main dosimetric peak, suggesting the onset of partial depletion of deeper traps; therefore, 145 °C represents an optimal compromise between efficient shallow-trap removal and preservation of the dosimetric signal integrity.

To evaluate the thermal duration required for effective trap depletion, the sample was preheated at the fixed temperature of 145 °C for varying durations ranging from 1 to 23 s. As shown in Fig. 3c, the integrated intensity remained approximately constant up to 9 s, beyond which a slight downward trend was noted, suggesting potential onset of deeper trap annealing. Therefore, a duration of 9 s was chosen to balance efficient removal of unstable traps without compromising deeper trap retention.

The final glow curve obtained under this preheating condition (145 °C for 9 s) is shown in Fig. 3d. Compared to the initial profile, this curve exhibits a smoother and more resolved peak structure, confirming the selective elimination of shallow traps and the thermal stability of the remaining signal. Notably, the TL response is dominated by a single well-defined glow peak centered at approximately 210 °C, indicating that the preheating protocol effectively isolates the main dosimetric trap. This preheating protocol was adopted for all subsequent TL measurements throughout this study.

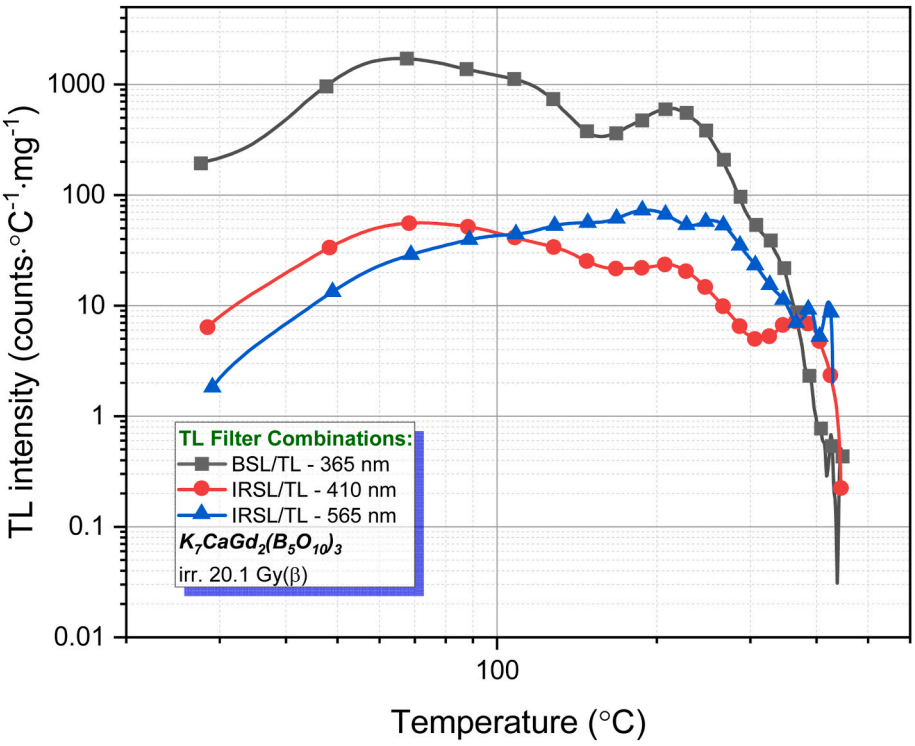

Fig. 2. Log–log TL glow curves of undoped $K_7CaGd_2(B_5O_{10})_3$ recorded after β-irradiation (20.1 Gy). The strongest emission corresponds to near-UV detection, suggesting dominant recombination in this spectral region.

3.4. Dose–response characteristics

To evaluate the dosimetric potential of undoped $K_7CaGd_2(B_5O_{10})_3$, TL glow curves were recorded over a broad β-dose range (1.4–500.8 Gy) following preheating at 145 °C for 9 s. As shown in Fig. 4a, the glow curve shape remains remarkably stable across all doses, with the main peak consistently centered around ~200 °C. No systematic shift in T_m was observed within experimental uncertainty (±2 °C), suggesting a stable trapping structure and negligible thermal quenching, both of which are essential for reproducible dosimetry.

According to TL theory, such peak stability is characteristic of near-first-order behaviour of an individual glow peak, where the peak temperature (T_m) remains largely independent of dose. This behaviour was first described by Kristianpoller et al. (1974), who showed that in simple kinetic systems, T_m remains dose-invariant unless retrapping or complex trap competition occurs. Our results align well with this theoretical expectation, indicating that the dominant dosimetric peak in $K_7CaGd_2(B_5O_{10})_3$ can be reasonably approximated by first-order kinetics under the investigated dose range.

To further validate the dose–response behaviour, the main peak intensity (I_{max}) was analyzed as a function of β-dose. I_{max} represents the contribution of the dominant recombination process. The dose dependence of the TL response was therefore evaluated using the peak height (I_{max}), which provides a direct and sensitive measure of the dosimetric signal. The peak height (Fig. 4b) exhibits a wide dynamic range and an approximately linear behaviour ($b \approx 1$) in the low-dose region (1.4–30.1 Gy), followed by a slight supralinear trend at higher doses. It is important to distinguish between the kinetic behaviour of the dominant peak and the global dose–response of the multi-trap system. While the invariance of T_m supports a near-first-order approximation for the dominant peak, the overall dose–response reflects weak interactions within the broader trapping–recombination network. Within the investigated dose range, no saturation behavior was observed. The TL response remains approximately linear at low doses and shows a slight supralinear trend at higher doses, with no evidence of signal saturation up to the maximum applied dose of 500.8 Gy. Power-law fits ($I = a \cdot D^b$) show excellent agreement ($R^2 > 0.998$). Separate nonlinear least-squares regressions were applied to the low-dose (1.4–30.1 Gy) and higher-dose regions. In the low-dose region, the fitted exponent was $b = 1.06 \pm 0.01$, indicating near-linear behaviour. In the higher-dose region, $b = 1.29 \pm 0.01$, reflecting a slight supralinear tendency. The reported uncertainties correspond to the regression-derived standard errors of the fitted exponent.

Each dose point represents a single-aliquot measurement; therefore, no statistical error bars are shown in Fig. 4b. The quoted uncertainties reflect fitting errors rather than measurement repeatability.

It is important to distinguish between the kinetic behaviour of the dominant peak and the global dose–response of the multi-trap system. While the invariance of T_m supports a near-first-order approximation for the dominant peak, the overall dose–response reflects weak interactions within the broader trapping–recombination network. Within the investigated dose range, no saturation behavior was observed up to the maximum applied dose of 500.8 Gy, indicating that exhaustion of the relevant trapping and luminescence centers is not reached within the studied β-dose range (Bos, 2001).

The slight supralinearity at higher doses may be attributed to increased interaction probability among occupied traps and competing recombination centers, as commonly discussed in interaction-based TL models (Abdel-Razek, 2016; Konstantinidis et al., 2020).

Overall, the retention of glow-curve shape and the approximately linear dose–response within the investigated β-dose range (1.4–500.8 Gy) indicate stable TL behaviour under the present experimental conditions. These findings suggest that the material may be considered for further investigation in intermediate-to high-dose β-irradiation applications within the studied regime. However, sub-Gy performance, photon-energy dependence, inter-aliquot reproducibility, and benchmarking against established dosimetric standards were not addressed in the present study and require systematic evaluation before broader dosimetric applicability can be established.

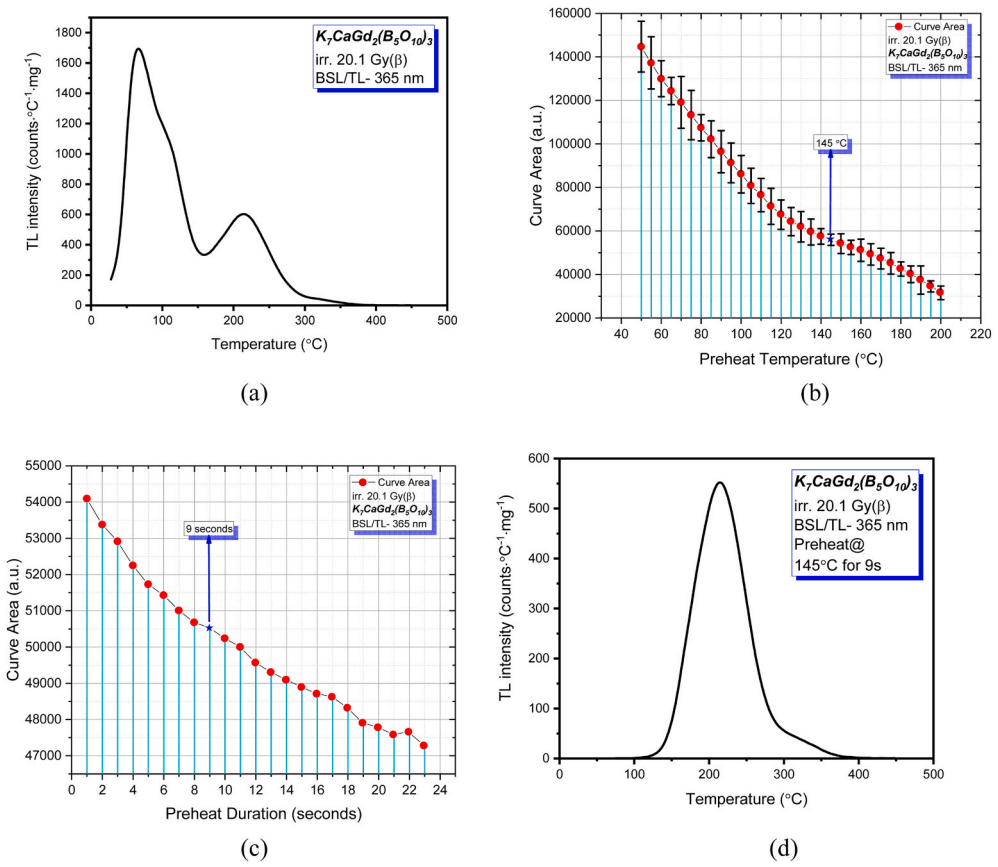

Fig. 3. (a) Initial TL glow curve of undoped $K_7CaGd_2(B_5O_{10})_3$ recorded without preheating, showing multiple low-temperature features. (b) Integrated TL intensity as a function of preheat temperature. A sharp decrease in intensity is observed up to 145 °C, followed by a markedly reduced rate of signal loss at higher preheat temperatures, indicating effective depletion of shallow traps. (c) Curve area vs. preheat duration at 145 °C. Signal remains stable up to 9 s, supporting this as the optimal hold time. (d) TL glow curve after optimized preheating (145 °C for 9 s), showing improved peak resolution and thermal stability.

3.5. Reusability and readout cycle stability

The potential of a TL phosphor for practical dosimetry applications relies not only on sensitivity and linearity, but also on the material's ability to maintain consistent response under repeated use. To assess this, undoped $K_7CaGd_2(B_5O_{10})_3$ samples were subjected to ten consecutive irradiation–readout cycles using a fixed β-dose of 20.1 Gy. Between each cycle, a standardized thermal annealing protocol was employed to ensure complete signal erasure and trap resetting.

Fig. 5a illustrates the TL glow curves obtained from each readout cycle, showing exceptional reproducibility in both shape and intensity. To quantify performance, Fig. 5b presents the total TL emission—expressed as integrated area—normalized to the first readout. Across all ten cycles, the signal deviation remained within ±0.38%, with the standard deviation falling well below the generally accepted ±5% limit for dosimetric reliability (Altowyan et al., 2024). The reusability test was performed on a single pellet (single aliquot), which was re-irradiated prior to each readout cycle under identical experimental conditions. Therefore, the reported variation reflects cycle-to-cycle reproducibility for the same aliquot rather than inter-aliquot variability. Error bars representing the standard deviation have been added to Fig. 5b to provide a transparent assessment of measurement repeatability.

Moreover, the position of the main glow peak (~210 °C) exhibited negligible shift ($\Delta T_m < 1.5$ °C) throughout all readouts, confirming the thermal and structural stability of the active trapping and recombination centers. This invariance in peak temperature supports the assertion that no significant trap redistribution or reconfiguration occurs during high-temperature annealing or multiple excitation cycles.

Together, these findings demonstrate that undoped $K_7CaGd_2(B_5O_{10})_3$ exhibits outstanding cycle-to-cycle stability, with minimal signal fading, negligible structural degradation, and excellent thermal resilience. Such robustness is critical in operational scenarios requiring repeated reuse of dosimeters without the need for recalibration, supporting the potential reusability of the material under the present readout–annealing protocol. Inter-aliquot reproducibility and performance under different radiation qualities require further study.

3.6. Anomalous heating rate effects in $K_7CaGd_2(B_5O_{10})_3$: deviations from classical TL kinetics

To further explore the TL behaviour of $K_7CaGd_2(B_5O_{10})_3$, glow curves were recorded across a range of linear heating rates (0.1–10 °C/s) following fixed preheating (145 °C for 9 s) and β-irradiation at 20.1 Gy. As illustrated in Fig. 6a, increasing the heating rate results in a progressive shift of the glow peak maximum toward higher temperatures, a behaviour fully consistent with classical TL kinetics. Specifically, the main dosimetric peak migrates from approximately 174 °C at 0.1 °C/s to ~250 °C at 10 °C/s, reflecting the expected thermal lag and increased temperature required to depopulate traps under rapid heating conditions. It should be noted that thermal lag primarily influences the apparent peak temperature (T_m) and does not inherently account for systematic variations in integrated TL intensity.

A quantitative evaluation of the temperature lag correction is presented in Fig. 6b. The lag effect is negligible at low heating rates (0.1–0.5 °C/s), where ΔT remains below ~2 °C. Even up to 2 °C/s, the correction does not exceed ~2 °C and does not significantly affect the extracted kinetic parameters. However, at higher heating rates (≥5 °C/

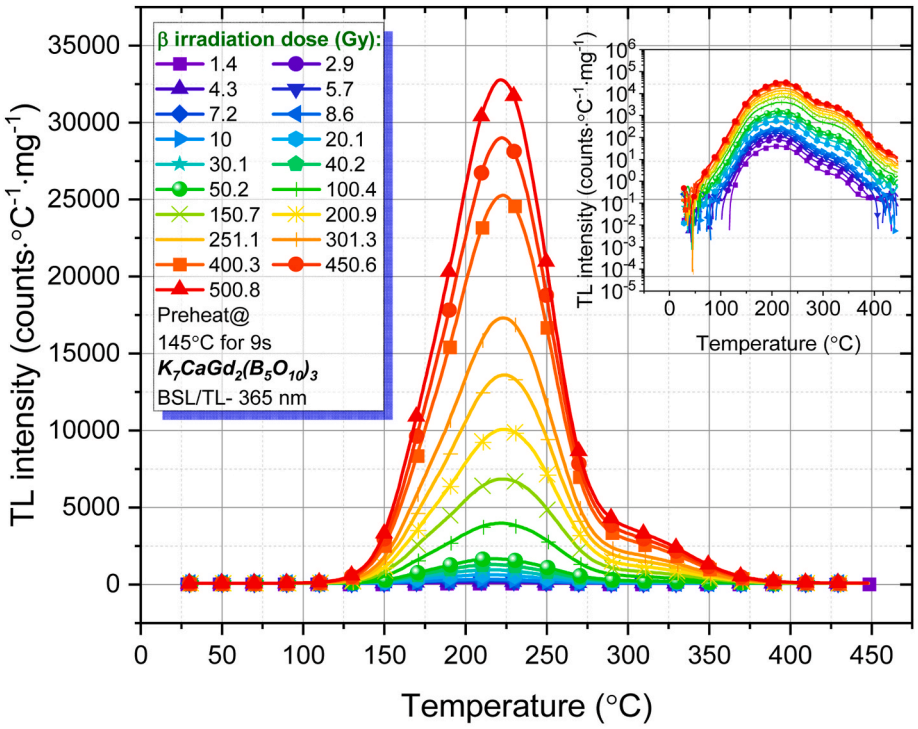

(a)

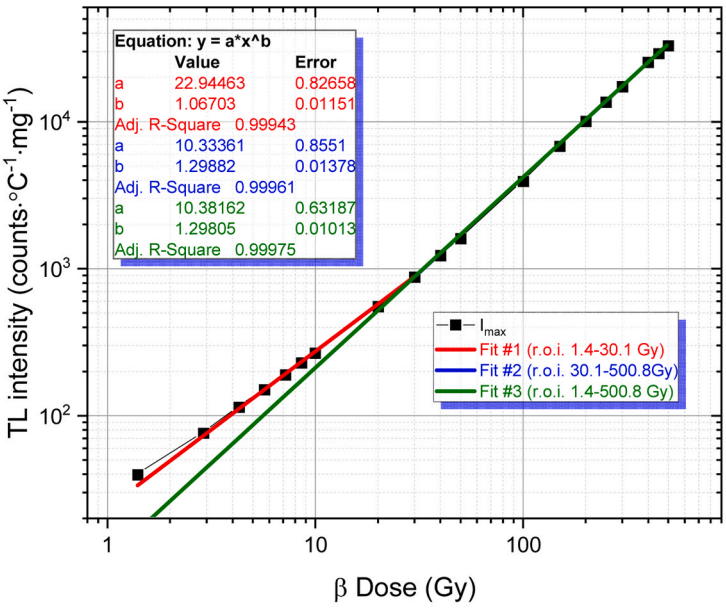

(b)

Fig. 4. (a) TL glow curves of undoped $K_7CaGd_2(B_5O_{10})_3$ recorded after β-irradiation at various doses (1.4–500.8 Gy). (b) Dose–response curve based on peak height. Power-law fits indicate supralinear and linear regimes.

s), the lag effect becomes progressively more pronounced, reaching ~14 °C at 10 °C/s. Importantly, the intensity enhancement discussed below is already observable within the low heating-rate regime where thermal lag is minimal. Therefore, the heating-rate-dependent intensity increase cannot be solely attributed to instrumental temperature delay effects.

Therefore, while the peak shift follows classical expectations, the intensity behaviour must be considered separately.

However, despite the conventional peak shift, a notable intensity enhancement is also observed with increasing heating rate—a phenomenon not accounted for by classical first- or general-order TL theories. According to standard models, TL intensity should remain constant or even decrease at higher heating rates due to reduced thermal contact time and possible incomplete recombination. To quantitatively assess this trend, Fig. 6c shows the normalized TL glow curve area as a function of heating rate, highlighting the non-classical heating-rate

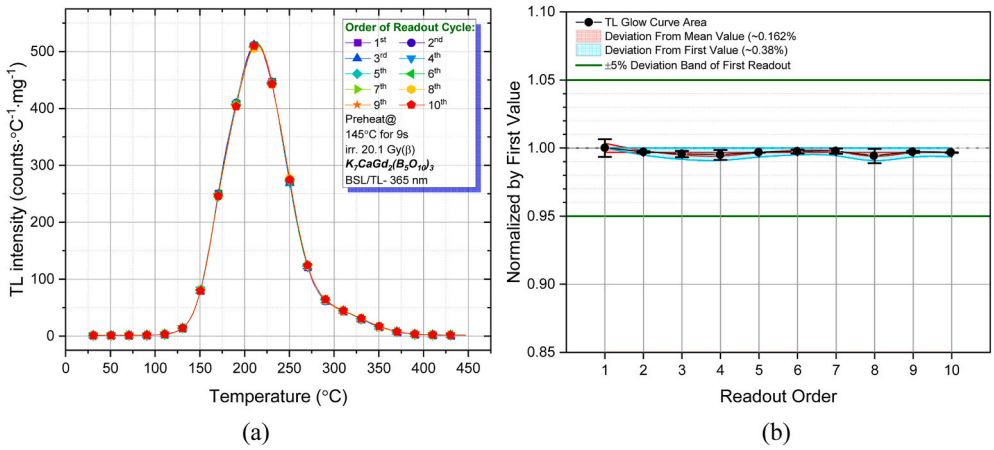

Fig. 5. (a) TL glow curves of undoped $K_7CaGd_2(B_5O_{10})_3$ over ten consecutive irradiation–readout cycles (20.1 Gy, preheat at 145 °C for 9 s), showing excellent reproducibility and thermal stability.(b) Normalized integrated TL intensity vs. readout order, demonstrating minimal deviation from the first readout (±0.38%) and high reusability within ±5% acceptance limits.

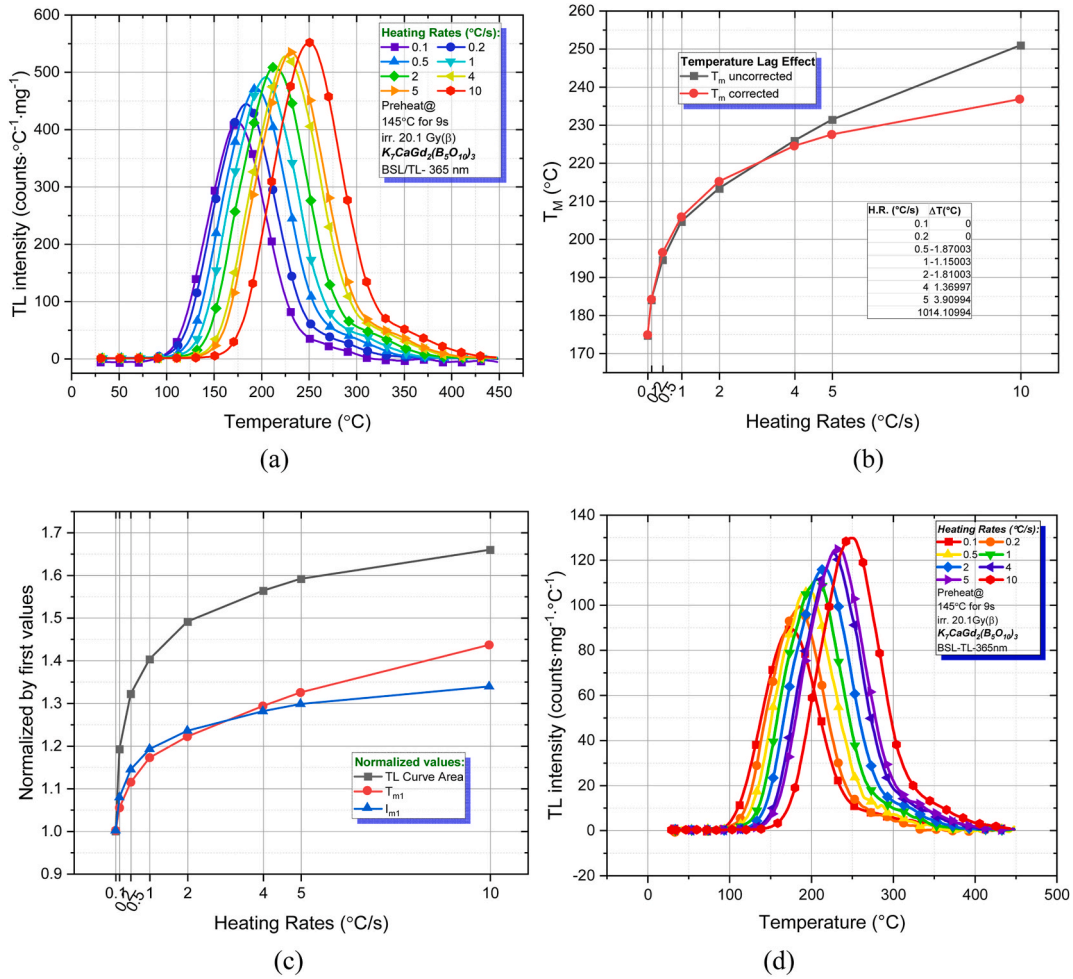

Fig. 6. (a) Normalized TL parameters of $K_7CaGd_2(B_5O_{10})_3$ as a function of heating rate. TL curve area shows a continuous and nonlinear increase with rising heating rates, indicating a systematic heating-rate-dependent increase in TL intensity. (b) Normalized TL glow curve area and corresponding peak temperature (T_{m1}) as a function of heating rate (0.1–10 °C/s). (c) Temperature lag effect in $K_7CaGd_2(B_5O_{10})_3$: variation of uncorrected and lag-corrected peak temperature (T_m) as a function of heating rate (0.1–10 °C/s), showing increasing ΔT at higher heating rates. (d) TL glow curves of $K_7CaGd_2(B_5O_{10})_3$ recorded at different heating rates (0.1–10 °C s^{-1}) for a second independently prepared aliquot under identical β-irradiation (20.1 Gy) and preheating (145 °C for 9 s) conditions.

dependence of the TL response. The total TL signal displays a consistent upward trend, increasing by approximately 66% from 0.1 to 10 °C/s. This trend indicates a partial anomalous heating-rate effect, wherein intensity increases systematically with thermal ramping in a manner not predicted by ideal first- or general-order kinetic models. The marked amplification of TL signal at elevated rates is consistent with an

anomalous heating-rate response, rather than a purely classical kinetic behaviour.

All heating-rate measurements were performed on the same aliquot under identical β-irradiation conditions. The reported ~66% increase refers to the relative change in integrated TL intensity for this single-aliquot dataset; no multi-aliquot statistical averaging was applied. The enhancement trend was reproducible under repeated heating-rate scans, indicating that it is unlikely to arise from random measurement fluctuation. Importantly, the intensity increase is already observable within the low heating-rate regime (0.1–0.5 °C/s), where thermal lag remains below ~2 °C and instrumental temperature-delay effects are negligible. While a dedicated reference-material comparison was not performed in the present study, the systematic nature of the observed trend suggests that the effect is unlikely to originate solely from heating-rate-dependent electronic gain variations of the TL reader.

The anomalous increase of integrated TL intensity with heating rate was reproduced on an independently prepared pellet, which exhibited a qualitatively similar trend in both peak shift and area–β dependence (Fig. 6c and d), confirming that the effect is not specific to a single aliquot.

This behaviour has been reported in several previous studies and remains a subject of active theoretical interest. Seminal works by Mandowski and Bos (2011) and Pagonis et al. (2013) introduced explanations based on semi-localized transition (SLT) models, suggesting that recombination efficiency itself is modulated by the rate of temperature increase. Additional studies have confirmed similar anomalies in diverse phosphors, including $LaCa_4O(BO_3)_3$:Eu^{3+}, $YAl_3(BO_3)_4$:Eu^{3+}, ZnB_2O_4:Gd^{3+}, $GdAl_3(BO_3)_4$:Sm^{3+}, and Ga_2S_3 crystals (Alajlani et al., 2025; Atasöz et al., 2022; Bulcar et al., 2025; Guler et al., 2018; Jabali et al., 2024; Souadi et al., 2023). These studies converge on the notion that recombination probabilities are not purely thermally driven, but also depend on charge carrier dynamics during the heating ramp.

It is important to distinguish between temperature-shift behaviour and intensity behaviour under varying heating rates. While the peak position follows classical TL expectations and remains consistent with near-first-order characteristics of the dominant trap, the heating-rate-dependent intensity amplification reflects additional dynamic processes beyond the simple kinetic approximation. In the case of $K_7CaGd_2(B_5O_{10})_3$, the TL response exhibits behaviour that may be described as a partial anomalous regime. While the glow peak position obeys classical thermal kinetics, the intensity behavior is anomalous, suggesting that recombination dynamics may be influenced under faster heating ramps. Possible contributing factors include reduced retrapping probability or enhanced carrier mobility; however, the present study does not directly resolve the microscopic mechanism. These interpretations should therefore be regarded as phenomenological explanations consistent with the observed glow-curve evolution rather than definitive structural conclusions. As heating rate increases, the TL peaks evolve from broader, asymmetric profiles (at 0.1–0.5 °C/s) to sharply defined, symmetric peaks (at 5–10 °C/s), as clearly visible in the glow curves. This narrowing may reflect a concentration of recombination events over a narrower temperature window, reflecting a kinetically coherent recombination regime.

From a dosimetric standpoint, this dual behaviour presents both opportunities and challenges. From a dosimetric standpoint, this dual behaviour presents both opportunities and constraints. Intensity amplification may enhance readout sensitivity under controlled heating conditions; however, the rate-dependent nonlinearities require careful calibration to ensure reproducible dosimetric performance, particularly in high-throughput or automated systems. Ultimately, the heating rate-dependent response of $K_7CaGd_2(B_5O_{10})_3$ reveals a complex kinetic structure that warrants further investigation through isothermal decay analysis or modelling within the SLT framework to fully elucidate the underlying processes.

4. Thermoluminescence kinetic analysis of the main dosimetric peak

4.1. Evaluation via variable heating rate (VHR) method

To quantitatively determine the kinetic parameters of the main dosimetric TL peak (~175 °C), a variable heating rate (VHR) approach was employed using two widely recognized methodologies: the Booth-Bohun-Parfianovitch (Bohun, 1954; Booth, 1954) method and the refined Hoogenstraaten method (Hoogensraaten, 1958). Glow curves were recorded over heating rates ranging from 0.1 to 10 °C/s, with and without temperature lag correction, and the activation energy E was extracted by plotting $ln(T_m^2/\beta)$, versus $1/(k_B T_m)$ where T_m is the glow peak temperature and β is the heating rate.

As presented in Fig. 7, both corrected and uncorrected data yield linear fits with excellent correlation ($R^2 \approx 0.99$), confirming the validity of the first-order approximation for the peak in question. The slope of the fitted lines directly yields the activation energy, while the intercept allows determination of the frequency factor s using the Hoogenstraaten relation (Alajlani et al., 2025; Souadi et al., 2025):

$$E = k \cdot \frac{T_{m1} T_{m2}}{T_{m1} - T_{m2}} \cdot ln\left(\frac{\beta_1}{\beta_2} \cdot \left(\frac{T_{m2}}{T_{m1}}\right)^2\right) \quad (1)$$

where k is the Boltzmann constant, T_{m1} is TL peak temperature using lowest heating rate value β_1, here it is 0.1 °C/s. T_{m2} is the TL peak temperature value observed for heating rate β_2.

In the variable heating rate framework, the activation energy can be extracted by comparing glow peak temperatures obtained at different heating rates. This approach relies on the sensitivity of the peak position to the heating rate and is particularly effective when the dominant glow peak follows near first-order kinetics. In practice, however, the accuracy of this analysis may be compromised by thermal lag effects, which arise from the finite heat transfer between the heater and the phosphor sample during readout.

At elevated heating rates, the actual sample temperature tends to lag behind the programmed temperature, leading to systematic shifts in the measured peak temperature Tm. If uncorrected, this effect can introduce non-negligible errors into the calculated kinetic parameters. To minimize such deviations, a temperature lag adjustment was applied prior to the kinetic evaluation, following the procedure proposed by Kitis and Tuyn (1998). This correction aligns the peak temperatures obtained at different heating rates onto a consistent thermal scale, thereby

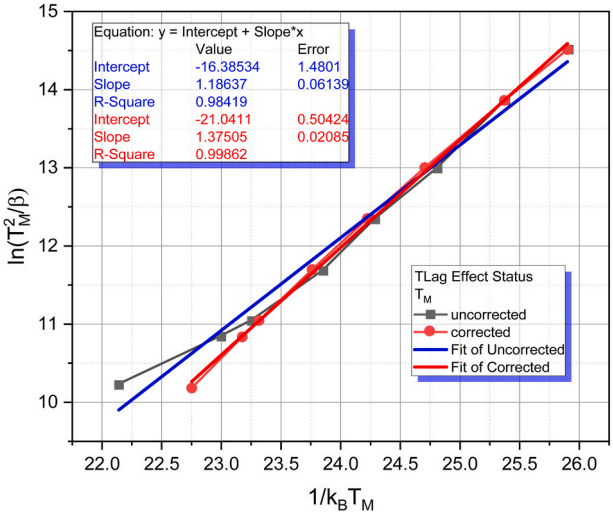

Fig. 7. Plot of ln (T_m^2/β) versus $1/k_BT_m$ used for the estimation of activation energy (E) of the main dosimetric TL peak in $K_7CaGd_2(B_5O_{10})_3$, employing both uncorrected and temperature lag-corrected peak temperatures.

improving the reliability of the activation energy and frequency factor determined from the VHR analysis.

The resulting activation energies, presented in Table 1, show excellent agreement between methods. The Booth-Bohun-Parfianovitch method yielded an average E of 1.28 ± 0.08 eV (uncorrected) and 1.31 ± 0.05 eV (corrected), while the Hoogenstraaten method (Hoogensraaten, 1958) gave values of 1.18 ± 0.06 eV and 1.37 ± 0.02 eV, respectively. The calculated frequency factors were 1.79×10^{11} s^{-1} and 2.19×10^{13} s^{-1}, suggesting fast recombination kinetics and good thermal stability. The elevated frequency factor estimated via Hoogenstraaten's method suggests a highly probable thermal escape process, indicating shallow retrapping and rapid recombination under readout conditions. The close agreement and low standard deviations observed between the two methods further suggest that the dominant dosimetric peak originates from a well-defined, homogeneously distributed trap center. This interpretation is consistent with a uniform trapping depth and implies a stable recombination environment. This consistency across methods also supports the view that the main dosimetric peak is governed by a single, kinetically coherent trap population. The VHR analysis assumes first-order kinetics for the purpose of extracting activation energies from the ln (Tm^2/β)–1/Tm relation. In the present study, this approximation is applied specifically to the dominant dosimetric peak. The corresponding ln (Tm^2/β)–$1/T_m$ plots, obtained from both temperature-lag-corrected and uncorrected datasets, exhibit highly linear behaviour ($R^2 \approx 0.99$), supporting the validity of a near-first-order approximation for this particular trap under the measurement conditions.

Importantly, this local kinetic approximation does not imply that the entire trapping–recombination system follows classical first-order behaviour. While the main dosimetric peak behaves quasi-independently and satisfies first-order criteria (Tm invariance and linear VHR response), the global TL response exhibits non-classical features. These include a pronounced heating-rate-dependent increase in total TL intensity (~66% from 0.1 to 10 °C/s) and a measurable post-irradiation signal enhancement (~20 fold after 12 h storage), both of which deviate from conventional first-order expectations.

Thus, first-order kinetics is assigned only to the dominant peak for parameter extraction, whereas the broader trap–recombination network demonstrates semi-localized and interaction-driven processes requiring non-classical interpretation. There is therefore no contradiction between the local first-order behaviour of the main dosimetric trap and the global non-classical dynamics of the system. This distinction between local kinetic approximation and global non-classical behaviour is essential for avoiding apparent inconsistencies in the interpretation of the TL data.

As will be discussed in Section 4.3, complementary CGCD analysis reveals that the overall TL signal comprises multiple glow peaks with distinct kinetic parameters. This indicates that, while the principal dosimetric component arises from a uniform and dominant trap, the material contains a broader distribution of trap levels contributing to the composite luminescence response.

These results indicate a robust trapping center responsible for the main dosimetric peak and demonstrate the necessity of temperature lag correction, particularly when high heating rates are used. Such corrections not only improve parameter accuracy but also reinforce the reliability of VHR-based TL kinetic analyses in $K_7CaGd_2(B_5O_{10})_3$.

Table 1
Calculated activation energy (E) and frequency factor (s) values for the main TL peak in $K_7CaGd_2(B_5O_{10})_3$ using Booth–Bohun–Parfianovitch and Hoogenstraaten methods with and without temperature lag correction.

β (°C/s)	*Maximum*		
	UnCorrecred	*Corrected*	
0.2	1.23	1.23	Booth-Bohun-Parfianovitch
0.5	1.38	1.26	Method
1	1.33	1.29	
2	1.37	1.31	
4	1.30	1.34	
5	1.26	1.35	
10	1.13	1.37	
Average E	**1.28 ± 0.08**	**1.31 ± 0.05**	
***E* (eV) (0.2–10 °C/s)**	**1.18 ± 0.06**	**1.37 ± 0.02**	Hoogenstraaten's Method
***s* (s^{-1})**	1.79×10^{11}	2.19×10^{13}	

4.2. T_m–T_{stop} experiment and initial rise (IR) method

To elucidate the distribution and nature of trapping centers in $K_7CaGd_2(B_5O_{10})_3$, the T_m–T_{stop} protocol in conjunction with the initial rise (IR) method was applied, as described by McKeewer (Garlick and Gibson, 1948; McKeever, 1985), and further adapted in recent works (Karmakar, 2012). This approach enables selective exploration of TL emission associated with traps of increasing depth by systematically raising the stopping temperature (T_{stop}) prior to glow curve acquisition. As T_{stop} increases, shallower traps are thermally depleted, and deeper traps dominate the remaining TL signal, allowing for a trap-resolved kinetic analysis.

In the IR method, the activation energy (E_a) is derived from the initial portion of the glow curve, where TL intensity (I) follows an exponential dependence on temperature (T), expressed as:

$$I(T) \propto exp\left(\frac{-E_a}{kT}\right) \quad (2)$$

Plotting ln(I) against 1/kT for the early rising edge of the glow peak (typically up to 10–15% of I_m) yields a linear relationship, from which the slope allows determination of E_a (Furetta and Weng, 1998). Fig. 8a presents the set of glow curves obtained after incremental T_{stop} values ranging from 50 °C to 335 °C, recorded prior to any preheating treatment, showing progressive suppression of the main dosimetric peak and the emergence of deeper peaks. Fig. 8b shows a T_m–T_{stop} evolution pattern based on glow curves measured before preheating, which bears strong similarity to previously reported behaviors in $Li_2B_4O_7$:Cu, Ag (Benavente et al., 2020) and LaB_3O_6:Tb^{3+} (Portakal-Uçar et al., 2023) systems, where distinct kinetic regimes and trap distributions were also observed. This pattern can be divided into four distinct regions:

(i) a linear rise from ~50 to 120 °C, indicating a continuum of shallow traps;
(ii) a stable plateau (~120–210 °C), typically associated with a general-order kinetic peak;
(iii) a second linear rise (~210–275 °C), suggesting another group of deeper traps with a quasi-continuous distribution;
(iv) a final gradual increase beyond 275 °C, pointing to high-stability trap centers.

Such segmentation into kinetic regions is consistent with the interpretation of quasi-continuous and discrete trapping distributions proposed in earlier studies, where linear and plateau behaviors in T_m–T_{stop} plots have been attributed to general-order kinetics and distributed trap systems (Benavente et al., 2020; McKeever, 1980).

Fig. 8c plots the activation energy E_a extracted from IR analysis of glow curves acquired without preheating, as a function of T_{stop}, revealing a staircase-like profile that signifies discrete trapping levels rather than a smooth continuum. Thirteen discrete trap levels were identified, with activation energies ranging from approximately 1.17 eV to 2.09 eV. This energy span is comparable to that reported in LaB_3O_6:Tb^{3+} (Portakal-Uçar et al., 2023), further validating the robustness of the IR method in mapping trap distributions across complex TL systems.

To further explore the thermal stability of the identified trapping levels, the T_m–T_{stop} protocol combined with the IR method was also

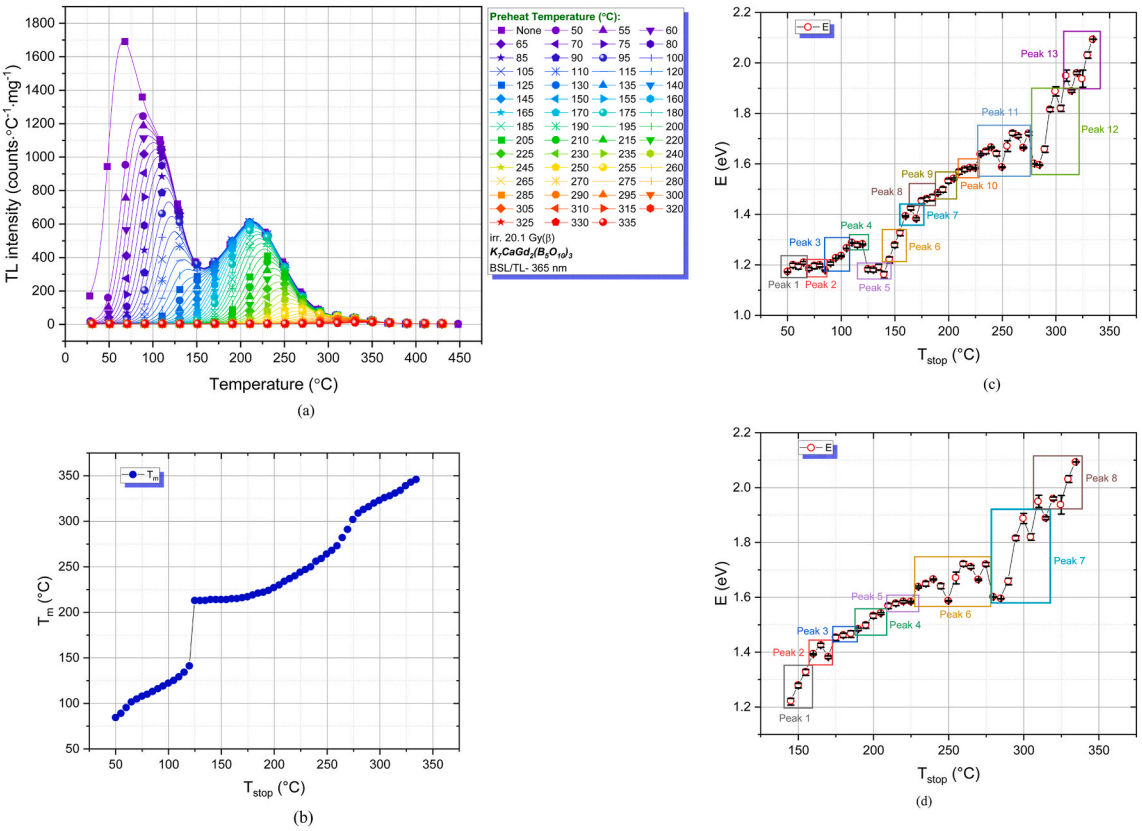

Fig. 8. (a) TL glow curves of $K_7CaGd_2(B_5O_{10})_3$ recorded following incremental T_{stop} treatments (50–335 °C) applied prior to glow curve acquisition, illustrating the progressive depletion of shallow traps and the emergence of deeper trapping components. (b) Evolution of T_m as a function of T_{stop}, showing multiple kinetic regions. (c) Activation energy (E_a) values extracted via the initial rise method across T_{stop} steps. (d) Post-preheating E_a–T_{stop} plot, highlighting deeper and more stable traps after thermal cleaning.

applied after the preheating treatment, targeting the deeper, thermally stable traps remaining in the system. Fig. 8d illustrates the evolution of activation energy (E_a) as a function of T_{stop} under these conditions. Compared to the preheating-free dataset (Fig. 8c), the post-preheating curve exhibits a narrower distribution of trap depths, ranging primarily between ~1.6 and 2.1 eV. This confirms that shallow and unstable traps below ~1.5 eV were effectively emptied during preheating, isolating a more robust subset of deeper traps. The resulting E_a–T_{stop} trend reveals a smoother, less segmented profile, reflecting a thermally cleaned trap population that may be more appropriate for long-term dosimetric applications requiring high signal stability. The complementary use of IR analysis before and after preheating thus enables a more comprehensive characterization of the trapping landscape in $K_7CaGd_2(B_5O_{10})_3$.

These IR results suggest the existence of multiple trapping levels with distinct activation energies, as evidenced by the stepwise increase in E_a with T_{stop}. Moreover, the consistency of E_a evolution with the segmented behavior in the T_m–T_{stop} plot strengthens the interpretation that the material exhibits both discrete and distributed kinetic components — a hallmark of materials with rich and hierarchical trap structures (Benavente et al., 2020). The identification of thirteen discrete trap depths points to a complex trap distribution, rather than a singular, well-defined trap. This diversity in trapping centers reinforces the multifaceted nature of the TL emission in $K_7CaGd_2(B_5O_{10})_3$.

While the main dosimetric peak appears to stem from a relatively uniform and kinetically stable trap—consistent with earlier VHR-based findings (see Section 4.2), the broader trap structure revealed by IR and T_m–T_{stop} analyses emphasizes the importance of pre-characterization prior to CGCD application, as also suggested by Portakal-Uçar et al. (2023). This layered kinetic behavior may offer practical advantages for dosimetric applications, especially in contexts demanding a broad dynamic range and high thermal stability.

A more detailed assessment of individual glow peak characteristics and their kinetic parameters will be provided in the following section through computerized glow curve deconvolution (CGCD) analysis.

4.3. CGCD analysis

In wide band-gap insulating materials, multiple trapping centers may coexist within the forbidden energy region, each potentially giving rise to a distinct TL peak. In practice, however, experimentally recorded TL glow curves rarely consist of isolated peaks; instead, they are typically formed by several partially overlapping components originating from traps with closely spaced activation energies. Consequently, the measured glow curve represents a superposition of multiple TL processes rather than a single kinetic event.

Glow Curve Deconvolution (CGCD) is therefore an essential analytical tool to disentangle these overlapping contributions and to extract reliable kinetic parameters associated with individual trapping centers. In the present study, CGCD was intentionally applied to TL glow curves recorded both *before* and *after* preheating treatment in order to elucidate the role of shallow and thermally unstable traps and to isolate the contribution of deeper, more stable trapping centers. The deconvolution analysis was carried out using the *tgcd* package implemented in the R statistical computing environment, an open-source program specifically designed for TL glow-curve analysis (Peng et al., 2016).

The deconvolution procedure was performed assuming general-order kinetics (GOK), expressed by Eq. (3) (M Gómez Ros and Kitis, 2002):

$$I(T) = I_m \exp\left(\frac{E}{kT_m^2}(T - T_m)\right)\left[\frac{1}{b} + \frac{b-1}{b}\exp\left(\frac{E}{kT_m^2}(T - T_m)\right)\right]^{-\frac{b}{b-1}} \quad (3)$$

Fig. 9a presents the CGCD analysis of the TL glow curve of the $K_7CaGd_2(B_5O_{10})_3$ sample recorded without preheating after 20.1 Gy beta irradiation. In this case, the glow curve was successfully decomposed into thirteen overlapping TL peaks, indicating the presence of a broad and quasi-continuous distribution of trapping centers extending from shallow to deep energy levels.

Importantly, the number of deconvolved components was not arbitrarily selected but was constrained by the independent T_m–T_{stop} and initial-rise (IR) analyses, which revealed multiple discrete activation-energy regions spanning approximately 1.17–2.09 eV. Thus, the CGCD analysis was guided by experimentally derived kinetic information rather than purely mathematical fitting freedom. It should be emphasized that the thirteen components represent a parametric description of a complex and partially overlapping trap distribution, rather than thirteen completely independent microscopic trapping centers.

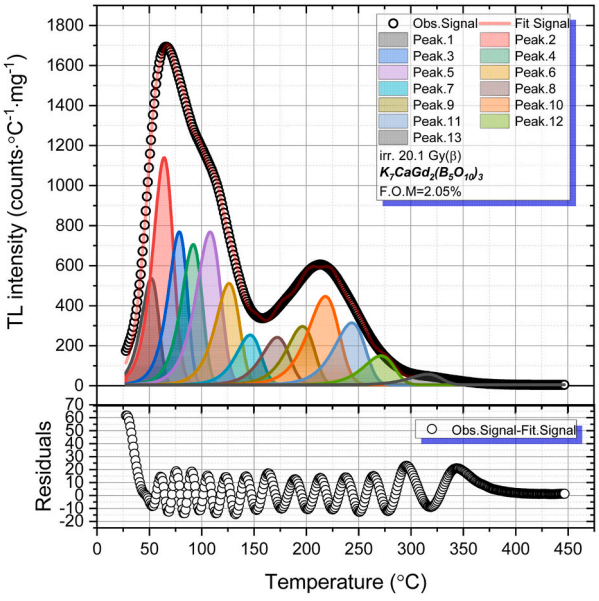

(a)

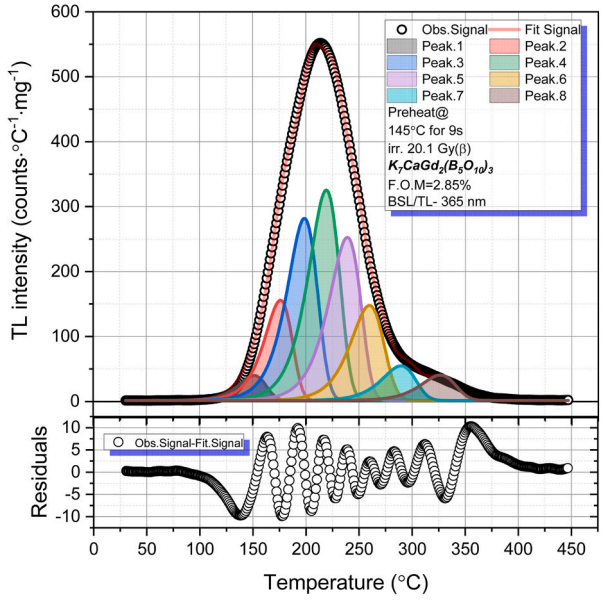

(b)

Fig. 9. CGCD analysis of TL glow curves of $K_7CaGd_2(B_5O_{10})_3$ phosphor irradiated with (a) 20.1 Gy β dose (b) after preheating at 145 °C for 9.

To evaluate fitting stability, repeated CGCD analyses were performed using varied initial parameter sets. The extracted activation energies and kinetic parameters (E_a, b, and s) exhibited relative variations below 4% across repeated runs, while the FOM remained below 3%, indicating stable convergence of the multi-peak solution. Therefore, thirteen components represent the smallest number of peaks that yields residuals without systematic structure and activation energies consistent with the independent IR and T_m–T_{stop} constraints, within the experimental resolution of the glow curve.

Repeated CGCD analyses were performed using varied initial parameter sets to evaluate fitting stability. The extracted activation energies and kinetic parameters (E_a, b, and s) exhibited relative variations below 4% across repeated runs, while the FOM remained below 3%, indicating stable convergence of the multi-peak solution.

Based on this stability analysis, the typical uncertainty in the activation energies is estimated to be within ±3–5%, corresponding approximately to ±0.03–0.07 eV depending on trap depth.

Frequency factors (s) exhibit comparatively larger intrinsic uncertainty due to parameter correlation in general-order kinetics; however, their relative variation across repeated fits remained below 4%, supporting the internal consistency of the extracted trap distribution.

The corresponding kinetic parameters for these thirteen components are listed in Table 2. It should be noted that the relatively high frequency factors obtained for several deconvoluted peaks are not anomalous and have been widely discussed in the TL literature. While early TL models associated the frequency factor with lattice vibrational frequencies (typically ~10^{12}–10^{13} s^{-1}), this assumption is valid primarily for models involving carrier transport through the conduction band. In systems where the trapping and recombination centers form a closely linked or composite defect complex, the apparent frequency factor may increase

Table 2
Trap parameters derived from CGCD analysis of the glow curve of $K_7CaGd_2(B_5O_{10})_3$ before preheating. Uncertainty in E_a estimated as ±0.03–0.07 eV based on repeated fitting stability analysis. Relative uncertainty in s is within one order of magnitude.

•	E_a (eV)	b	T_m (°C)	T_{m1} (°C)	T_{m2} (°C)	μ	s (s^{-1})
1st Peak	1.19	1.12	52.27	40.71	60.59	0.43	6.96×10^{17}
2nd Peak	1.20	1.30	64.57	51.72	74.65	0.42	1.94×10^{17}
3rd Peak	1.26	1.08	79.05	66.39	87.97	0.42	2.51×10^{17}
4th Peak	1.28	1.15	92.44	78.78	102.43	0.43	9.73×10^{16}
5th Peak	1.19	1.16	108.64	92.59	120.44	0.41	9.58×10^{14}
6th Peak	1.32	1.14	126.86	111.05	138.36	0.42	8.12×10^{15}
7th Peak	1.42	1.17	147.01	130.69	159.07	0.42	1.99×10^{16}
8th Peak	1.46	1.20	172.96	154.94	186.47	0.42	5.25×10^{15}
9th Peak	1.54	1.08	197.16	178.70	210.18	0.42	5.11×10^{15}
10th Peak	1.58	1.19	219.07	198.84	234.15	0.42	2.25×10^{15}
11th Peak	1.72	1.13	244.443	224.17	259.11	0.43	8.27×10^{15}
12th Peak	1.88	1.11	272.40	251.90	287.09	0.42	3.39×10^{16}
13th Peak	2.09	1.07	316.99	295.63	331.98	0.41	9.78×10^{16}

by several orders of magnitude.

Yazan et al. (2021) demonstrated that such high s values ($\geq 10^{16}$–10^{20} s^{-1}) naturally arise when the trap and luminescence centers are spatially correlated, allowing direct or semi-localized transitions rather than long-range carrier transport through the lattice. In such configurations, the frequency factor no longer represents a simple lattice vibrational attempt frequency but instead reflects the probability of thermally assisted escape within a coupled defect configuration. Accordingly, elevated *s* values are interpreted as signatures of efficient and spatially correlated recombination pathways. Therefore, the high frequency factors obtained in the present CGCD analysis support the presence of closely associated trapping–recombination centers and are consistent with the observed thermal stability of the deeper TL peaks.

The extracted activation energies span a wide range, reflecting the coexistence of thermally unstable shallow traps together with intermediate and deep traps. Such complexity is characteristic of TL glow curves obtained without thermal cleaning, where low-temperature peaks associated with shallow traps significantly overlap with higher-temperature components. For the preheated sample, Fig. 9b illustrates the corresponding CGCD analysis, confirming the selective removal of shallow traps and the dominance of deeper, thermally stable peaks. The extracted trap depths were found to lie between ~1.32 and 2.09 eV, with corresponding peak temperatures systematically shifted toward higher values (Table 3). The resulting figure of merit (FOM) of 2.85% indicates a reliable and physically meaningful deconvolution, remaining within the generally accepted confidence range for CGCD analyses (Balian and Eddy, 1977; Misra and Eddy, 1979). The calculated frequency factors fall within ~10^{14}–10^{16} s^{-1}, consistent with thermally stimulated detrapping processes in insulating borate-based phosphor materials. High frequency factors ($s > 10^{16}$–10^{20} s^{-1}) have been extensively reported in rare-earth-doped insulating systems and are not inherently unphysical.

The comparative CGCD results obtained before and after preheating provide direct insight into the thermal stability of the trapping centers. While the non-preheated glow curve reflects a complex mixture of shallow and deep traps, the preheated glow curve isolates the contribution of deeper traps with longer lifetimes. This distinction is crucial for applications requiring stable signal retention, as shallow traps contribute primarily to short-term TL response, whereas deeper traps govern long-term storage and delayed emission behavior.

Overall, the strong consistency between CGCD, the initial-rise method, and the T_m–T_{stop} analysis confirms that the extracted kinetic parameters are experimentally constrained and physically meaningful. The deliberate application of CGCD both before and after preheating thus provides a thermally controlled validation of the trap distribution and minimizes the likelihood of unconstrained overfitting.

Table 3
Trap parameters obtained from CGCD analysis of the glow curve of $K_7CaGd_2(B_5O_{10})_3$ after preheating at 145 °C for 9 s. Uncertainty in E_a estimated as ±0.03–0.07 eV based on repeated fitting stability analysis. Relative uncertainty in s is within one order of magnitude.

•	E_a (eV)	*b*	T_m (°C)	T_{m1} (°C)	T_{m2} (°C)	μ	*s* (s^{-1})
1st Peak	1.32	1.14	151.85	134.01	164.83	0.42	7.56×10^{14}
2nd Peak	1.42	1.07	176.75	158.47	189.57	0.40	1.30×10^{15}
3rd Peak	1.46	1.11	199.38	179.57	213.57	0.43	5.62×10^{14}
4th Peak	1.54	1.09	219.98	199.64	234.41	0.41	8.01×10^{14}
5th Peak	1.58	1.04	239.84	218.65	254.46	0.40	4.6×10^{14}
6th Peak	1.72	1.13	260.65	239.10	276.25	0.41	2.41×10^{15}
7th Peak	1.88	1.12	290.36	268.43	306.15	0.43	8.89×10^{15}
8th Peak	2.09	1.15	327.50	304.94	344.01	0.41	4.58×10^{16}

4.4. Anomalous time-dependent TL enhancement in $K_7CaGd_2(B_5O_{10})_3$: departure from classical fading behaviour

To evaluate the temporal evolution of the TL signal in $K_7CaGd_2(B_5O_{10})_3$, a time-dependent stability study was conducted by recording TL glow curves at various storage times after β-irradiation. As shown in Fig. 10a, the glow curves measured at time intervals from 0 s to 12 h reveal a non-classical behaviour: instead of the expected signal decay typically associated with fading, the main glow peak centered at approximately 220 °C exhibits a gradual and measurable increase in intensity. This observation is inconsistent with conventional TL fading models, which generally predict monotonic signal loss due to the thermal or quantum-mechanical instability of shallow traps (McKeever, 1985; Bos, 2001). This enhancement is further quantified in Fig. 10b, where the integrated TL intensity shows a consistent upward trend, with the signal increasing by over a 20-fold enhancement after 12 h of room temperature storage.

As shown in Fig. 10c, the normalized integrated TL intensity (I/I_0) remains nearly constant during the initial storage period (up to ~10^3 s), indicating negligible short-term fading or sensitivity drift. The data points represent the mean values obtained from four independently prepared pellets (n = 4), with standard deviation error bars.

At longer storage times, however, a pronounced enhancement of the TL signal is observed. The normalized intensity increases progressively and reaches approximately a 20–30-fold amplification after 12 h of room-temperature storage. Such a magnitude of post-irradiation signal growth deviates from classical fading expectations, where a monotonic decrease in signal intensity would normally be anticipated.

It is important to emphasize that the instrumental reproducibility of the TL system was previously verified to remain within ±0.38% over ten consecutive irradiation–readout cycles (Section 3.5). The magnitude of the observed amplification therefore exceeds the experimental uncertainty by more than two orders of magnitude and cannot be attributed to simple readout instability or global sensitivity drift.

At the present stage, the exact microscopic origin of this pronounced enhancement cannot be unambiguously determined. Delayed recombination processes, tunnelling-assisted transfer, or trap-to-trap charge redistribution are proposed here as physically plausible interpretations consistent with non-classical TL models, rather than definitive mechanistic assignments.

Such behavior deviates markedly from classical fading dynamics and points toward a *time-dependent signal amplification* process rather than simple trap depletion.

The observed 20-fold enhancements post-irradiation intensity increase therefore significantly exceeds the experimental uncertainty and cannot be attributed to simple sensitivity drift or readout instability.

A qualitatively similar phenomenon, explicitly referred to as *inverse fading*, has recently been reported for both TL and OSL signals in NaCl-based dosimetric materials by Ekendahl et al. (2025). Inverse fading has also been reported previously in NaCl-based luminescent systems, where the OSL signal was observed to increase by up to 50% over several weeks after irradiation (Waldner and Bernhardsson, 2018). In that study, the luminescence signal increased systematically with storage time over periods extending from days to months after irradiation. Importantly, the authors demonstrated that this inverse fading behavior is reproducible, observable across different detector preparations, and intrinsic to the material, thereby excluding trivial experimental artefacts.

The observation of inverse fading in other dosimetric systems such as NaCl demonstrates that time-dependent signal enhancement has been reported in TL materials, and therefore the present behaviour cannot be dismissed a priori as a measurement artefact. A plausible explanation for this phenomenon involves delayed recombination pathways mediated by spatially correlated defect structures. In particular, tunnelling-

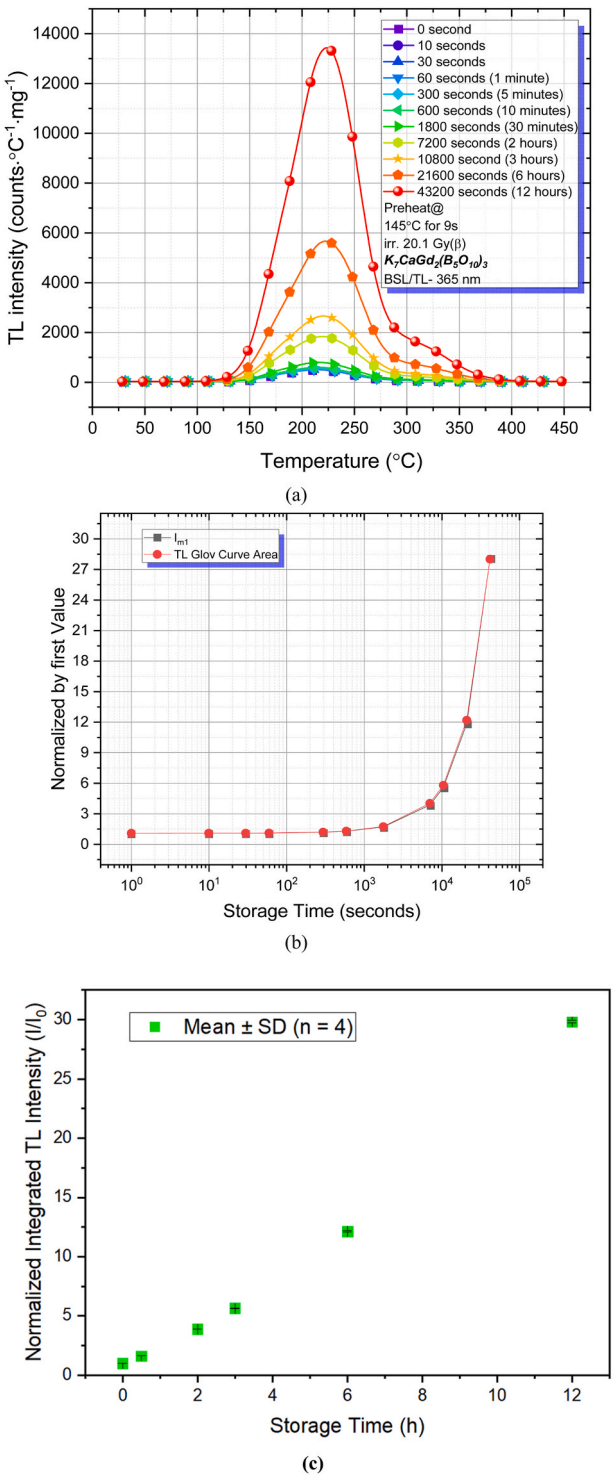

Fig. 10. (a) TL glow curves of $K_7CaGd_2(B_5O_{10})_3$ recorded at various storage times after β-irradiation. (b) Normalized TL signal as a function of storage time for $K_7CaGd_2(B_5O_{10})_3$ (c) Normalized integrated TL intensity (I/I_0) of $K_7CaGd_2(B_5O_{10})_3$ as a function of storage time after β-irradiation. The signal exhibits a pronounced time-dependent enhancement, reaching ~20 times the initial value after 12 h. Error bars represent ±1 SD (n = 4).

assisted recombination has been proposed in other complex insulating systems as a mechanism for time-dependent luminescence evolution. Recent work by Pagonis et al. (2020) demonstrated that in feldspar systems, TL is dominated by tunnelling-assisted recombination between randomly distributed donor–acceptor pairs. Their Monte Carlo simulations and experimental analysis showed that recombination can occur without thermal activation and that TL signals may evolve over time as trapped charge carriers tunnel across potential barriers to neighboring recombination centers. These tunnelling-based models demonstrate that non-thermally activated recombination pathways can influence the temporal evolution of luminescence signals in certain materials. Although no direct post-irradiation TL enhancement was reported in feldspars, the tunnelling models developed by Pagonis et al. (2020) offer a plausible mechanism for delayed recombination processes that can lead to non-classical temporal signal evolution.

Further support for this interpretation can be drawn from detailed fading studies performed on α-Al_2O_3:C and α-Al_2O_3:C, Mg (Kalita and Chithambo, 2017a, 2017b). In α-Al_2O_3:C,Mg, significant fading of the main peak was attributed to electron migration via shallow traps, where charge hopping and tunnelling-assisted transfer between spatially correlated defect centers were proposed as dominant mechanisms. In contrast, α-Al_2O_3:C exhibited inverse fading behaviour of its main dosimetric peak, which was associated with delayed charge redistribution and gradual filling of recombination-efficient configurations. These findings demonstrate that both fading and inverse fading phenomena can originate from redistribution processes within a multiple interacting trapping level from simple thermal instability of isolated traps.

In this context, the post-irradiation TL enhancement observed in $K_7CaGd_2(B_5O_{10})_3$ can be interpreted within a similar framework of charge redistribution and spatially correlated recombination dynamics. The gradual increase in TL intensity during storage suggests that a fraction of carriers initially occupy metastable or weakly coupled trapping states and subsequently migrate—either via tunnelling-assisted transfer or thermally assisted hopping—toward energetically or spatially more favourable recombination centers. This interpretation is consistent with previously documented phenomenology in established dosimetric systems and therefore should be regarded as physically plausible rather than purely speculative.

At the present stage, the exact microscopic mechanism cannot be unambiguously determined. Tunnelling-assisted transfer and trap-to-trap charge redistribution are proposed here as physically plausible interpretations consistent with established TL models, rather than definitive mechanistic assignments. The reproducibility of the inverse-fading-like behaviour and the absence of conventional signal loss are consistent with, but do not prove, an intrinsic contribution from the trapping–recombination system of $K_7CaGd_2(B_5O_{10})_3$, although direct structural confirmation remains beyond the scope of the present study. Further investigations, including isothermal decay and time-resolved studies, will be required to discriminate between competing microscopic scenarios.

In addition to the mechanisms discussed above, alternative explanations should also be considered. A gradual change in intrinsic sensitivity during storage could, in principle, mimic an inverse-fading-like enhancement. However, the excellent cycle-to-cycle stability (±0.38%) and the invariant peak temperature ($\Delta T_m < 1.5$ °C) observed in Section 3.5 argue against a simple global sensitivity drift as the dominant origin of the effect.

Activation or stabilization of recombination centers during storage may also enhance recombination efficiency over time. While the present data do not directly resolve recombination-center dynamics, the stability of the glow-curve structure suggests that no major reconfiguration of the primary trap–recombination framework occurs.

Structural relaxation effects within a complex defect network cannot be excluded and may contribute to gradual modifications in trap–center spatial relationships. However, the current dataset does not allow unambiguous separation of these possibilities. Therefore, tunnelling-assisted transfer and charge redistribution are proposed here as physically plausible interpretations consistent with established TL models, rather than definitive mechanistic assignments.

5. Conclusion

TL glow curve analysis revealed a broad and complex structure, indicative of multiple trapping centers spanning a wide energy range. Detailed kinetic characterization employing various complementary techniques—including Variable Heating Rate (VHR), Initial Rise (IR), and Computerized Glow Curve Deconvolution (CGCD) provided a model-dependent decomposition into thirteen resolvable components, with activation energies ranging from approximately 1.17 to 2.09 eV and frequency factors reaching up to 10^{20} s^{-1}. These parameters are consistent with a complex trapping landscape and may reflect coupled or spatially associated trap–recombination configurations, although alternative interpretations cannot be excluded.

The application of a preheating protocol enabled the selective removal of unstable shallow traps, enhancing the resolution of deeper TL components and further validating the thermal robustness of the stable trapping sites. Following preheating, the material exhibited eight well-resolved peaks (E_a = 1.32–2.09 eV), including a dominant dosimetric peak centered at ~220 °C. Within the investigated β-dose interval (1.4–500.8 Gy), the material exhibited stable and approximately linear behaviour in the low-to-intermediate region, with slight supralinearity at higher doses. This assessment is restricted to the studied dose range. A particularly intriguing finding was the reproducible time-dependent TL enhancement observed within 12 h of storage, representing deviation from conventional monotonic fading expectations. This inverse fading–like behaviour, previously reported only in limited material systems, may be associated with delayed recombination, tunnelling-mediated processes, or charge redistribution among metastable traps. Furthermore, the material exhibited non-classical heating rate behavior, whereby TL intensity increased continuously and nonlinearly with rising heating rates, deviating from standard kinetic expectations. Such behaviour is consistent with the possible involvement of semi-localized or dynamically evolving recombination pathways beyond conventional first-order descriptions. Taken together, the structural characterization and kinetic analyses suggest that K7CaGd2(B5O10)3 may serve as a suitable system for exploring deviations from ideal first-order TL behaviour and time-dependent charge relaxation phenomena. Additionally, robust X-ray diffraction (XRD) data confirmed high phase purity and crystallinity, providing a solid structural foundation for the observed TL phenomena. Overall, this study contributes to the understanding of deep trapping states, non-classical TL kinetics, and inverse fading–like behaviour in complex borate-based phosphors, clarifying the kinetic diversity that can arise even in undoped systems. The present dosimetric evaluation is limited to β irradiation within the range 1.4–500.8 Gy. Low-dose (<1 Gy) sensitivity, minimum detectable dose, and photon energy dependence were not examined in this study and require further investigation before broader dosimetric applications can be established.

CRediT authorship contribution statement

E. Aymila Cin: Methodology, Investigation, Formal analysis. **Kenan Bulcar:** Methodology, Investigation, Formal analysis. **Abeer S. Altowyan:** Writing – original draft, Methodology, Investigation, Funding acquisition, Formal analysis. **M.B. Coban:** Methodology, Investigation. **U.H. Kaynar:** Methodology, Investigation, Formal analysis. **O.T. Ozmen:** Methodology, Investigation. **Jabir Hakami:** Software, Methodology, Investigation. **H. Aydin:** Methodology, Investigation. **A. Canimoglu:** Methodology, Investigation. **Mustafa Topaksu:** Methodology, Investigation. **N. Can:** Writing – review & editing, Writing – original draft, Supervision, Conceptualization.

Declaration of competing interest

The authors declare that they have no known competing financial interests or personal relationships that could have appeared to influence the work reported in this paper.

Acknowledgements

The authors acknowledge the Princess Nourah bint Abdulrahman University Researchers Supporting Project (Project No. PNURSP2026R16), Princess Nourah bint Abdulrahman University, Riyadh, Saudi Arabia. This work was also supported by the Scientific and Technological Research Council of Turkey (TUBITAK, project number: 1001-223M036).

Data availability

Data will be made available on request.

References

Abdel-Razek, Y.A., 2016. Thermoluminescence dosimetry using natural calcite. J. Taibah Univ. Sci. 10, 286–295. https://doi.org/10.1016/j.jtusci.2015.08.002.

Alajlani, Y., Oglakci, M., Barad, A., Kaynar, U.H., Topaksu, M., Canimoglu, A., Can, N., 2025. Anomalous heating rate and kinetic analysis in the thermoluminescence of GdCa4O(BO3)3. Radiat. Phys. Chem. 232, 112614. https://doi.org/10.1016/j.radphyschem.2025.112614.

Alathlawi, H.J., Barad, A., Madkhali, O., Souadi, G., Sharahili, M., Hakami, J., Balci, S., Kaynar, U.H., Topaksu, M., Can, N., 2025. Intrinsic thermoluminescence and anomalous heating rate effects in undoped K7SrY2(B5O10)3 phosphors: a combined Tm–Tstop and GOK deconvolution study. Appl. Radiat. Isot. 225, 112092. https://doi.org/10.1016/j.apradiso.2025.112092.

Altowyan, A.S., Sonsuz, M., Kaynar, U.H., Hakami, J., Portakal-Uçar, Z.G., Ayvacikli, M., Topaksu, M., Can, N., 2024. Synthesis and thermoluminescence behavior of novel Sm3+ doped $YCa_4O(BO_3)_3$ under beta irradiation. Ceram. Int. 50, 19681–19691. https://doi.org/10.1016/j.ceramint.2024.03.089.

Atasöz, S., Topaksu, M., Souadi, G., Can, N., 2022. Anomalous heating rate dependence and analyses of thermoluminescence glow curves in Gd doped ZnB_2O_4 phosphors. J. Lumin. 246, 118838. https://doi.org/10.1016/j.jlumin.2022.118838.

Bakr, M., Portakal-Uçar, Z.G., Yüksel, M., Kaynar, Ü.H., Ayvacikli, M., Benourdja, S., Canimoglu, A., Topaksu, M., Hammoudeh, A., Can, N., 2020. Thermoluminescence properties of beta particle irradiated $Ca_3Al_2O_6$ phosphor relative to environmental dosimetry. J. Lumin. 227, 117565. https://doi.org/10.1016/j.jlumin.2020.117565.

Balian, H.G., Eddy, N.W., 1977. Figure-of-merit (FOM), an improved criterion over the normalized chi-squared test for assessing goodness-of-fit of gamma-ray spectral peaks. Nucl. Instrum. Methods 145, 389–395. https://doi.org/10.1016/0029-554X(77)90437-2.

Benavente, J.F., Gómez-Ros, J.M., Correcher, V., 2020. Characterization of the thermoluminescence glow curve of $Li_2B_4O_7$:Cu,Ag. Radiat. Meas. 137, 106427. https://doi.org/10.1016/j.radmeas.2020.106427.

Bohun, A., 1954. Thermoemission und Photoemission von Natriumchlorid. Czech. J. Phys. 4, 91–93. https://doi.org/10.1007/BF01688114.

Booth, A.H., 1954. Calculation of electron trap depths from Thermoluminescence Maxima. Can. J. Chem. 32, 214–215. https://doi.org/10.1139/v54-027.

Bos, A.J.J., 2001. High sensitivity thermoluminescence dosimetry. Nucl. Instrum. Methods Phys. Res. Sect. B Beam Interact. Mater. Atoms 184 (1–2), 3–28. https://doi.org/10.1016/S0168-583X(01)00717-0.

Bulcar, K., Portakal-Uçar, Z.G., Zelai, T., Souadi, G., Hakami, O., Kaynar, U.H., Madkhali, O., Topaksu, M., Can, N., 2025. Undoped and Eu doped $LaCa_4O(BO_3)_3$ phosphors: thermoluminescence characteristics with a focus on kinetic parameters, anomalous heating rate, and dose response. Ceram. Int. 51, 1124–1142. https://doi.org/10.1016/j.ceramint.2024.11.094.

Can, N., Townsend, P.D., Wang, Y., 2025. Analytical benefits from logarithmic displays of luminescence sensitivity. Vacuum 238, 114273. https://doi.org/10.1016/j.vacuum.2025.114273.

Çin, E.A., Bulcar, K., Hakami, J., Kaynar, U.H., Sharahili, M., Madkhali, O., Somaily, D., Karmouch, R., Jabali, D.A., Coban, M.B., Price, G.M.G., Topaksu, M., Can, N., 2026. Thermoluminescence study of $YBa_3(BO_3)_3$: trap characterization and kinetic parameters via multi-method analysis. Ceram. Int. 52, 273–285. https://doi.org/10.1016/j.ceramint.2025.11.316.

Delice, S., Isik, M., Gasanly, N.M., 2019. Low temperature thermoluminescence of Gd_2O_3 nanoparticles using various heating rate and Tmax − Texc. methods. Results Phys. 12, 1809–1813. https://doi.org/10.1016/j.rinp.2019.02.025.

Dorenbos, P., 2003. Systematic behaviour in trivalent lanthanide charge transfer energies. J. Phys. Condens. Matter 15, 8417–8434. https://doi.org/10.1088/0953-8984/15/49/018.

Ekendahl, Daniela, Čemusová, Zina, Sofer, Zdeněk, Plutnarová, Iva, 2025. Thermoluminescence and optically stimulated luminescence dosimetry with NaCl detectors made at different sintering temperatures. Radiat. Meas. 184, 107443. https://doi.org/10.1016/j.radmeas.2025.107443.

Furetta, C., Weng, P.-S., 1998. Operational thermoluminescence dosimetry. World Scientific. https://doi.org/10.1142/3789.

Garlick, G.F.J., Gibson, A.F., 1948. The electron trap mechanism of luminescence in sulphide and silicate phosphors. Proc. Phys. Soc. 60, 574–590. https://doi.org/10.1088/0959-5309/60/6/308.

Grachev, B.G., Deĭgen, M.F., 1978. Electron-nuclear double resonance of impurity centers in nonmetallic crystals. Sov. Phys. Usp. 21, 674–692. https://doi.org/10.1070/PU1978v021n08ABEH005673.

Guler, I., Isik, M., Gasanova, L., Mahammadov, A., Gasanly, N., 2018. Thermoluminescence in gallium sesquisulfide single crystals: usual and unusual heating rate dependencies. Optik 165, 132–136. https://doi.org/10.1016/j.ijleo.2018.03.105.

Hai, N.T.Q., Anh, T.K., Ha, V.T.T., Chau, P.T.M., Tuyen, H. Van, Thanh, N.T., Minh, L.Q., 2018. UV light induced thermoluminescence of rare Earth doped nanomaterials Y_2O_3:Eu^{3+}, Gd_2O_3:Eu^{3+} and Gd_2O_3:Er^{3+}. Commun. Phys. 28, 75. https://doi.org/10.15625/0868-3166/28/1/10910.

Hayes, W., Stoneham, A.M., 2014. Defects and Defect Processes in Nonmetallic Solids. Dover Publications.

Hoogensraaten, W., 1958. Electron traps in ZnS phosphorus. Philips Res. Rep. 13, 515–613.

Jabali, D.A., Madkhli, A.Y., Souadi, G., Kaynar, Ü.H., Coban, M.B., Madkhali, O., Ayvacikli, M., Amri, N., Can, N., 2024. Temperature-responsive insights: investigating Eu^{3+} and Dy^{3+} activated yttrium calcium oxyborate phosphors for structure and luminescence. Appl. Radiat. Isot. 206, 111214. https://doi.org/10.1016/j.apradiso.2024.111214.

Kalita, J.M., Chithambo, M.L., 2017a. A comparative study of the dosimetric features of α-Al_2O_3:C,Mg and α-Al_2O_3:C. Radiat. Protect. Dosim. 177 (3), 261–271. https://doi.org/10.1093/rpd/ncx039.

Kalita, J.M., Chithambo, M.L., 2017b. On the sensitivity of thermally and optically stimulated luminescence of α-Al_2O_3:C and α-Al_2O_3:C,Mg. Radiat. Meas. 99, 18–24. https://doi.org/10.1016/j.radmeas.2017.03.006.

Karmakar, M., 2012. On the initial rise method for kinetic analysis in thermally stimulated luminescence. Indian J. Sci. Technol. 5, 1–4. https://doi.org/10.17485/ijst/2012/v5i11.18.

Kitis, G., Tuyn, J.W.N., 1998. A simple method to correct for the temperature lag in TL glow-curve measurements. J. Phys. D Appl. Phys. 31, 2065–2073. https://doi.org/10.1088/0022-3727/31/16/017.

Konstantinidis, P., Tsoutsoumanos, E., Polymeris, G.S., Kitis, G., 2020. Thermoluminescence response of various dosimeters as a function of irradiation temperature. Radiat. Phys. Chem. 177, 109156. https://doi.org/10.1016/j.radphyschem.2020.109156.

Kristianpoller, N., Chen, R., Israeli, M., 1974. Dose dependence of thermoluminescence peaks. J. Phys. D Appl. Phys. 7, 313. https://doi.org/10.1088/0022-3727/7/7/313.

Kuznetsov, A.B., Ezhov, D.M., Kokh, K.A., Kononova, N.G., Shevchenko, V.S., Uralbekov, B., Bolatov, A., Svetlichnyi, V.A., Lapin, I.N., Simonova, E.A., Kokh, A.E., 2019. Nonlinear optical crystals $K_7CaR_2(B_5O_{10})_3$ (R = Nd, Yb): growth and properties. J. Cryst. Growth 519, 54–59. https://doi.org/10.1016/j.jcrysgro.2019.05.007.

M Gómez Ros, J., Kitis, G., 2002. Computerised glow curve deconvolution using general and mixed order kinetics. Radiat. Protect. Dosim. 101, 47–52. https://doi.org/10.1093/oxfordjournals.rpd.a006029.

Madkhli, A.Y., Jabali, D.A., Souadi, G., Sonsuz, M., Kaynar, U.H., Akça-Özalp, S., Ayvacikli, M., Madkhali, O., Topaksu, M., Can, N., 2024. Beta irradiation-induced thermoluminescence: glow curve analysis and kinetic parameters in combustion-synthesized undoped $Ca_4YO(BO_3)_3$. Appl. Radiat. Isot. 208, 111301. https://doi.org/10.1016/j.apradiso.2024.111301.

Mandowski, A., Bos, A.J.J., 2011. Explanation of anomalous heating rate dependence of thermoluminescence in YPO_4:Ce^{3+},Sm^{3+} based on the semi-localized transition (SLT) model. Radiat. Meas. 46, 1376–1379. https://doi.org/10.1016/j.radmeas.2011.05.018.

McKeever, S.W.S., 1985. Thermoluminescence of Solids. Cambridge University Press. https://doi.org/10.1017/CBO9780511564994.

McKeever, S.W.S., 1980. On the analysis of complex thermoluminescence. Glow-curves: resolution into individual peaks. Phys. Status Solidi 62, 331–340. https://doi.org/10.1002/pssa.2210620139.

Misra, S.K., Eddy, N.W., 1979. IFOM, a formula for universal assessment of goodness-of-fit of gamma ray spectra. Nucl. Instrum. Methods 166, 537–540. https://doi.org/10.1016/0029-554X(79)90546-9.

Morsy, M.A., Garrison, T.F., Kessler, M.R., Mhareb, M.H.A., El-Deen, H.Z., 2025. Structural elucidation of lithium borate glasses using XRD, FTIR, and EPR spectroscopy. ACS Phys. Chem. Au 5, 227–238. https://doi.org/10.1021/acsphyschemau.4c00106.

Pagonis, V., Blohm, L., Brengle, M., Mayonado, G., Woglam, P., 2013. Anomalous heating rate effect in thermoluminescence intensity using a simplified semi-localized transition (SLT) model. Radiat. Meas. 51–52, 40–47. https://doi.org/10.1016/j.radmeas.2013.01.025.

Pagonis, V., Kitis, G., Polymeris, G.S., 2020. Quantum tunneling processes in feldspars: using thermoluminescence signals in thermochronometry. Radiat. Meas. 134, 106325. https://doi.org/10.1016/j.radmeas.2020.106325.

Peng, J., Dong, Z., Han, F., 2016. Tgcd: an R package for analyzing thermoluminescence glow curves. SoftwareX 5, 112–120. https://doi.org/10.1016/j.softx.2016.06.001.

Peng, J., Wang, X., Adamiec, G., Pagonis, V., Choi, J.-H., 2021. Modelling the dependence of equivalent dose determined from a dose recovery test on preheating temperature: the intervention of shallow electron traps. Radiat. Meas. 142, 106566. https://doi.org/10.1016/j.radmeas.2021.106566.

Portakal-Uçar, Z.G., Oglakci, M., Correcher, V., Sonsuz, M., Can, N., Halefoglu, Y.Z., Topaksu, M., 2023. A thermoluminescence study of Tb^{3+} doped LaB_3O_6: dosimetric characteristics and kinetic parameters. J. Lumin. 253, 119493. https://doi.org/10.1016/j.jlumin.2022.119493.

Souadi, G., Bulcar, K., Akça-Özalp, S., Kaynar, U.H., Alathlawi, H.J., Madkhali, O., Sharahili, M., Somaily, D.A.E., Topaksu, M., Can, N., 2025. Anomalous heating rate dependence and kinetic analysis of Eu^{3+}-activated $K_7SrY_2(B_5O_{10})_3$ borate phosphors. Ceram. Int. 51, 53432–53441. https://doi.org/10.1016/j.ceramint.2025.09.091.

Souadi, G., Kaynar, Ü.H., Sonsuz, M., Akça-Özalp, S., Ayvacikli, M., Topaksu, M., Ozmen, O.T., Can, N., 2023. Unravelling the impact of unusual heating rate, dose-response and trap parameters on the thermoluminescence of Sm^{3+} activated $GdAl_3(BO_3)_4$ phosphors exposed to beta particle irradiation. Radiat. Phys. Chem. 213, 111211. https://doi.org/10.1016/j.radphyschem.2023.111211.

Tawalare, P.K., 2022. Luminescent inorganic mixed borate phosphor materials for lighting. Luminescence 37, 1226–1245. https://doi.org/10.1002/bio.4301.

Terashima, K., Tamura, S., Kim, S., Yoko, T., 1997. Structure and nonlinear optical properties of lanthanide borate glasses. J. Am. Ceram. Soc. 80 (11), 2903–2909. https://doi.org/10.1111/j.1151-2916.1997.tb03210.x.

Ton, N.D., Luan, N.T., Cho, J.Y., Choi, E.J., Jeong, D.W., Daniel, D.J., Kim, H.J., Kothan, S., Kaewkhao, J., 2025. Comparative study on scintillation and luminescence of terbium-doped LaB_3O_6 crystalline and glass materials. J. Lumin. 288, 121510. https://doi.org/10.1016/j.jlumin.2025.121510.

Townsend, P.D., Wang, Y., 2024. Improving interpretations of imperfections in insulating materials for current technologies. Opt. Mater. X 22, 100327. https://doi.org/10.1016/j.omx.2024.100327.

Waldner, L., Bernhardsson, C., 2018. Physical and dosimetric properties of NaCl pellets made in-house for the use in prospective optically stimulated luminescence dosimetry applications. Radiat. Meas. 119, 52–57. https://doi.org/10.1016/j.radmeas.2018.09.001.

Yang, B., Townsend, P.D., Rowlands, A.P., 1998. Low-temperature thermoluminescence spectra of rare-earth-doped lanthanum fluoride. Phys. Rev. B 57, 178–188. https://doi.org/10.1103/PhysRevB.57.178.

Yazan, H., Portakal-Uçar, Z.G., Akça, S., Topaksu, M., Townsend, P.D., Can, N., 2021. Thermoluminescence of Ce and Nd co-doped CaF_2 phosphors after beta irradiation. J. Lumin. 234, 117949. https://doi.org/10.1016/j.jlumin.2021.117949.

Yin, L., Wang, Y., Pan, L., Zhang, M., Li, Y., Yang, J., Lu, X., Townsend, P.D., 2023. Tailored luminescence of Bi doped $Ca_3Ga_4O_9$ phosphors with the substitution of strontium ions. Opt. Mater. 139, 113737. https://doi.org/10.1016/j.optmat.2023.113737.

Yukihara, E.G., Bos, A.J.J., Bilski, P., McKeever, S.W.S., 2022. The quest for new thermoluminescence and optically stimulated luminescence materials: needs, strategies and pitfalls. Radiat. Meas. 158, 106846. https://doi.org/10.1016/j.radmeas.2022.106846.